PERGAMON

Progress in Aerospace Sciences 38 (2002) 389–420

PROGRESS IN AEROSPACE SCIENCES

www.elsevier.com/locate/paerosci

Review of research on low-profile vortex generators to control boundary-layer separation

John C. Lin*

Flow Physics and Control Branch, NASA Langley Research Center, Hampton, VA 23681-2199, USA

Abstract

An in-depth review of boundary-layer flow-separation control by a passive method using low-profile vortex generators is presented. The generators are defined as those with a device height between 10% and 50% of the boundary-layer thickness. Key results are presented for several research efforts, all of which were performed within the past decade and a half where the majority of these works emphasize experimentation with some recent efforts on numerical simulations. Topics of discussion consist of both basic fluid dynamics and applied aerodynamics research. The fluid dynamics research includes comparative studies on separation control effectiveness as well as device-induced vortex characterization and correlation. The comparative studies cover the controlling of low-speed separated flows in adverse pressure gradient and supersonic shock-induced separation. The aerodynamics research includes several applications for aircraft performance enhancement and covers a wide range of speeds. Significant performance improvements are achieved through increased lift and/or reduced drag for various airfoils—low-Reynolds number, high-lift, and transonic—as well as highly swept wings. Performance enhancements for non-airfoil applications include aircraft interior noise reduction, inlet flow distortion alleviation inside compact ducts, and a more efficient overwing fairing. The low-profile vortex generators are best for being applied to applications where flow-separation locations are relatively fixed and the generators can be placed reasonably close upstream of the separation. Using the approach of minimal near-wall protuberances through substantially reduced device height, these devices can produce streamwise vortices just strong enough to overcome the separation without unnecessarily persisting within the boundary layer once the flow-control objective is achieved. Practical advantages of low-profile vortex generators, such as their inherent simplicity and low device drag, are demonstrated to be critically important for many applications as well.
Published by Elsevier Science Ltd.

Contents

*Tel.: +1-757-864-5556; fax: +1-757-864-7897.
E-mail addresses: j.c.lin@larc.nasa.gov (J.C. Lin).

0376-0421/02/$ - see front matter Published by Elsevier Science Ltd.
PII: S0376-0421(02)00010-6

Nomenclature

A	wing aspect ratio
C_D	drag coefficient
C_{D0}	drag coefficient at zero lift
C_L	lift coefficient
C_p	pressure coefficient
CFD	computational fluid dynamics
c	reference airfoil chord
DC(60)	circumferential distortion descriptor (=maximum $(Pt_{ave} - Pt_{min})/q_{ave}$ in any 60.0° sector)
DERA	Defence Evaluation and Research Agency
DOE	design of experiment
e	device chord length for vane VGs; device length in streamwise direction for wedge, ramp, doublet, and wishbone VGs
h	device height
h_e	device effective height
h_e^+	non-dimensional effective height ($= u_\tau h/\nu$)
K	lift-dependent drag factor ($=(C_D\text{-}C_{D0})\pi A/C_L^2$)
L/D	lift-to-drag ratio
LE	leading edge
M	Mach number
MEMS	micro electrical mechanical systems
NASA	National Aeronautics and Space Administration
n	gap ratio of counter-rotating vanes
P	leading-edge flow-separation point on highly swept wing
PIV	particle image velocimetry
P_t	total pressure
P_{t_0}	inlet total pressure
P_w	wall static pressure
q	free-stream dynamic pressure
R	local test section radius
RANS	Reynolds-averaged Navier–Stokes
RMS	root-mean-square
Re	Reynolds number
Re_c	Reynolds number based on reference chord c
S_1	ordinary separation line on highly swept wing
S_2	leading-edge separation line on highly swept wing
TE	trailing edge
u, U	streamwise velocity
u_τ	friction velocity ($=(\tau_w/\rho)^{0.5}$)
VG	vortex generator
x, X	coordinate along the streamwise direction
y, Y	coordinate normal to the wall
y^+	y value in law-of-the-wall variable ($=yu_\tau/\nu$)
z	coordinate along the spanwise direction and parallel to the wall
α	airfoil or aircraft angle of attack
β	device angle of incidence; device half angle for wedge, ramp, wishbone, and one row of doublet VGs
Γ	vortex circulation
Δ	differential values
ΔX_{VG}	distance between the VG trailing edge and baseline separation line.
Δz	device spacing in the spanwise direction
δ	boundary-layer thickness (at the device location)
δ^*	boundary-layer displacement thickness
δ_{gf}	boundary-layer thickness of the gap flow over the flap
δ_o	undisturbed boundary-layer thickness at the shock location
θ	boundary-layer momentum thickness
ν	kinematic viscosity
ρ	density
τ_w	wall shear stress
ω_x	streamwise vorticity

Subscripts

0.5	value at 0.5 h downstream of the device trailing edge
5	value at 5 h downstream of the device trailing edge
ave	average value
d	aerodynamic interface plane (fan face) diameter or conditions
s	shock
max	maximum value
min	minimum value
t	device trailing edge
th	inlet throat value
∞	free-stream value

1. Introduction

Because of the large energy losses often associated with boundary-layer separation, flow-separation control remains extremely important for many technological applications of fluid mechanics [1–3]. Controlling flow separation can result in an increase in system performance with consequent energy conservation as well as weight and space savings. In addition, multidisciplinary issues increasingly play an important role in modern aircraft design. Competitive pressures in the civil-transport aircraft industry drive aircraft designers toward low-cost solutions, whereas combat aircraft have to operate efficiently over a wide range of conditions. This means compromises have to be made in aerodynamic design; thus, considerations must given for certain aircraft system configurations featuring flows that are either separated or close to separation. One practical solution lies in the use of flow-control devices to provide an expanding degree of freedom in the design optimization process.

Conventional, vane-type, passive vortex generators (VGs) with device height, h, on the order of the boundary-layer thickness, δ, have long been used to control flow separation by increasing the near-wall momentum through the momentum transfer from the outer (free-stream) flow to the wall region. First introduced by Taylor [4] in the late 1940s, these devices consisted of a row of small plates or airfoils that project normal to the surface and are set at an angle of incidence, β, to the local flow to produce an array of streamwise trailing vortices. These conventional VGs have been used to delay boundary-layer separation [5], to enhance aircraft wing lift [6,7], to tailor wing-buffet characteristics at transonic speeds [7,8], to reduce afterbody drag of aircraft fuselages [9], and to avoid or delay separation in subsonic diffusers [10]. A wide variety of conventional VGs are in use, and numerous aircraft successfully employ them for separation control. Many aerodynamics applications, however, use these relatively large (δ-scale) VGs to control a localized flow separation over a relative short downstream distance. These VGs may incur excess residual drag through conversion of aircraft forward momentum into unrecoverable turbulence in the aircraft wake. Therefore, a more efficient or optimized VG design could be achieved for certain applications where the separation location is fairly fixed and does not require covering a large downstream distance by the devices.

In the early 1970s, Kuethe [11] developed and examined non-conventional wave-type VGs with h/δ of 0.27 and 0.42 that use the Taylor–Goertler instability to generate streamwise vortices within the boundary layer when the fluid is directed to flow over a concave surface. These low-profile devices successfully reduce the intensity of acoustic disturbances in the wake region by suppressing the formation of the Kármán vortex street and reducing the area of velocity deficit in the wake [11]. From research performed in the late 1980s, an exploratory separation control study by Rao and Kariya [12] suggests that submerged VGs with $h/\delta \leqslant 0.625$ have the potential of exceeding the performance of conventional VGs with $h/\delta \sim 1$, because of the much lower device (or parasitic) drag. Subsequently, several researchers since then show that by using low-profile VGs with the device height only a fraction of the conventional vane-type VGs, these generators (i.e., $0.1 \leqslant h/\delta \leqslant 0.5$) can still provide sufficient wallward momentum transfer over a region several times their own height for effective flow-separation control. In addition to lower device drag, the low-profile VGs offer other advantages when compared with the larger conventional VGs because of their compact size, such as allowing the devices to be stowed within the wing when not needed (e.g., on slotted flaps) and lower radar cross section.

This paper provides an in-depth review of investigations in the past 15 years [13–36] that used low-profile VGs to control boundary-layer separation, from basic fluid dynamics research to several aerodynamics applications for performance enhancement. The basic research includes comparative effectiveness on flow-separation control at low speed [13–17] and supersonic [18,19] flows, as well as device parameter correlation and vortex characterization [20–23]. The aerodynamics applications include airfoil/wing performance improvements through increased lift and/or reduced drag for a low-Reynolds number airfoil [24], high-lift airfoils [25,26], highly swept wings [27–31], and a transonic airfoil [18]. The non-airfoil aerodynamics applications include aircraft interior noise reduction at transonic cruise [32], inlet flow distortion reduction within compact ducts [33–35], and a more efficient overwing fairing [36]. These flow-control applications may significantly benefit many civil transport aircraft as well as maneuverable and stealthy combat aircraft over a wide range of speeds from subsonic to supersonic. Low-profile VGs come in many shapes and sizes, but for this paper, low-profile VGs are classified as those VGs with a device height between 10% and 50% of the boundary-layer thickness. These low-profile (sub-δ-scale) VGs have also been referred to by several names from different references, such as submerged VGs [13–15,24], micro VGs [16,17,25,36], sub boundary-layer vortex generators (SBVGs) [20,21,27–30,32], MEMS-scale effectors [34], and microvanes [35]. Therefore, for consistency and clarity, they are referred to as "low-profile VGs" in this paper.

2. Basic fluid dynamics research

Basic fluid dynamics research for the low-profile VGs consists of two main categories. The first includes

investigations that focus on examining the effectiveness of devices for flow-separation control. The second includes those investigations that aim to provide characterization of device-induced vortical flowfield downstream mainly for the development of numerical simulations. A chronological summary of representative investigations for each category is presented in Tables 1 and 2. The tables provide summaries of important VG parameters such as VG type, h/δ, e/h (non-dimensional device length), β, $\Delta z/h$ (non-dimensional device spacing), and $\Delta X_{VG}/h$ (non-dimensional streamwise distance between VG trailing edge and baseline separation), which describe the device geometry, size, orientation, and location for effective flow control. The investigation of flow-control effectiveness consists of two subcategories of flow separation caused by adverse pressure gradients at low speeds and by normal shock at supersonic speeds (see Table 1). In-depth discussions of these comparative flow-control investigations are presented in Sections 2.1.1 and 2.1.2. These discussions include the beneficial results, the effective flow-control parameters, and the understanding of basic controlling mechanisms involved for the low-profile VGs. The key results for the vortex characterization, correlation, and CFD prediction are presented in Section 2.2 (see Table 2).

2.1. Comparative effectiveness in flow-separation control

2.1.1. Adverse pressure gradients in low speeds

The first research examples of basic flow-separation control studied are experiments conducted at the NASA Langley Research Center 20-in × 28-in Shear Flow Tunnel in the late 1980s. These studies examine flow-separation control over a two-dimensional (2D), 25°-sloped, backward-facing curved ramp at low speed ($U_\infty = 132$ ft/s) [13–16]. Numerous types of passive flow-control devices are examined and compared for their separation-control effectiveness. The most effective performance results for each device category are summarized in Fig. 1(a) as a function of the percent reduction in the separated-flow region. The figure indicates that the most effective group of flow-separation control devices was that which generated streamwise vortices, such as those produced by the low-profile VGs, conventional VGs, and large longitudinal surface grooves. The low-profile VGs (referred to as "submerged" VGs by Lin et al. [13–15] and as "micro VGs" by Lin [16]) examined include counter-rotating and co-rotating vane-type VGs as well as Wheeler's doublet and wishbone VGs (Fig. 1(b)). These low-profile VGs with $h/\delta \sim 0.2$ (sub-δ-scale) are just as effective in delaying separation as the conventional VGs with $h/\delta \sim 0.8$ (δ-scale). The second most effective group incorporates those devices that generate transverse vortices, such as those produced by spanwise cylinders, LEBU and elongated arches at $+10°$ angle of attack, Viets' flapper, and transverse grooves. These devices are generally less effective than the low-profile VGs, and because they required more complete spanwise coverage, they tend to incur higher form drag as well [14,16]. The drag reducing riblets have virtually no effect on flow separation, whereas the passive porous surfaces and swept grooves examined enhance separation.

To illustrate the benefit of low-profile VGs, Fig. 2 compares the oil-flow visualization results of baseline (Fig. 2(a)) with the "conventional" vane-type counter-rotating VGs (Fig. 2(b)). The conventional VGs examined are reported to have a $h/\delta \sim 0.8$ (rectangular shape, $e/h = 2$, $\Delta z/h = 4$, $\beta = \pm 15°$) and placed at approximately $6h$ ($\sim 5\delta$) upstream of the baseline separation (based on the device trailing edge). The results indicate that each pair of counter-rotating VGs provide mostly attached flow directly downstream of the ramp trailing edge (Fig. 2(b)). However, this attached flow is highly three-dimensional (3D) and pockets of recirculating flow are still seen on the separation ramp between adjacent attached-flow regions. This highly 3D nature of the downstream flow is also an indication that the vortices produced by the conventional VGs are stronger than necessary. Weaker vortices (smaller VGs) that produce just strong enough streamwise vortices to overcome the separation would be more efficient. This is demonstrated in Fig. 2(c) by placing vane-type "low-profile" counter-rotating VGs with $h/\delta = 0.2$ (rectangular shape, $e/h = 4$, $\Delta z/h = 9$, $\beta = \pm 25°$) at approximately $10h$ ($\sim 2\delta$) upstream of baseline separation. The low-profile VGs successfully reduce the extent of separation by almost 90% [16]. Unlike the conventional VGs, the low-profile VGs do not adversely affect separation-control effectiveness by generating excessively strong vortices that cause pockets of recirculating flow via the strong upsweep motion of vortices.

Streamwise pressure distributions for conventional and low-profile VGs are presented in Figs. 3(a) and (b), respectively. The figures show that the "inflection point" in the pressure rise of the VG-off baseline (solid line) corresponds roughly to where the boundary layer separates. For the VG cases, the surface pressures are measured at three spanwise locations (i.e., 0, $\Delta z/4$, $\Delta z/2$) along and downstream of the ramp (see Fig. 3). The results confirm the effectiveness of the low-profile VGs; they are observed to be just as effective in eliminating the inflection point, which is an indication that the separation has been significantly reduced, as with the conventional VGs. Fig. 3(b) shows not only significant improvement in downstream pressure recovery over the baseline, but also substantial reduction of variations between the three spanwise locations over the larger VGs. This is indicative of a greatly reduced "excess" 3D flow over the conventional VGs. Lin et al. [14] show that lowering h/δ of VGs from 0.2 to 0.1 reduces the

Table 1
Summary of research on boundary-layer flow-separation control effectiveness for low-profile VGs

Investigator(s) (Year pub.)	Test bed	Type of study	Flow parameters	VG type	Most effective VG parameters examined					Comments
					h/δ	e/h	$\Delta z/h$	β (deg)	$\Delta X_{VG}/h$	
Adverse gradients at low speeds										
Lin et al. (1990) [13]	Backward-facing ramp	Wind-tunnel test	$U_\infty = 132$ ft/s, $\delta = 1.28$ in	Doublets	0.1	~13	8	±25	20	Doublet VGs with $h/\delta \sim 0.1$ are most effective in separation control.
Lin et al. (1990) [14]; Lin et al. (1991) [15]	Backward-facing ramp	Wind-tunnel test	$U_\infty = 132$ ft/s, $\delta = 1.28$ in	Wishbones	0.2	~3	4	±23	10	Reverse Wishbone VGs with $h/\delta \sim 0.2$ are most effective in separation control.
Lin (1999) [16]	Backward-facing ramp	Wind-tunnel test	$U_\infty = 132$ ft/s, $\delta = 1.28$ in	Counter-rotating rectangular vanes	0.2	4	9	±25	10	Embedded stream-wise vortices produced by $h/\delta \sim 0.2$ counter-rotating vanes are most effective in 2D separation control.
Ashill et al. (2001) [20]	Bump	Wind-tunnel test	$U_\infty = 20$ m/s, $\delta = 33$ mm	Counter-rotating delta vanes	0.3	~10	12	±14	52	Counter-rotating vanes with $1\,h$ spacing are most effective in reducing the extent of separation region.
				Forward wedges	0.3	10	12	±14	52	
Jenkins et al. (2002) [17]	Backward-facing ramp	Wind-tunnel test	$U_\infty = 140$ ft/s, $\delta = 0.87$ in	Co-rotating trapezoid vanes	0.2	4	4	23	12 and 19	Low-profile VGs are the most effective device examined in controlling 3D flow-separation dominated by a pair of juncture vortices.
Supersonics shock-induced separation										
McCormick (1992) [18]	Shock-induced separation over flat plate	Wind-tunnel test	$M_\infty = 1.56$ to 1.65, $\delta_{VG} = 0.389$ cm	Doublets	0.36	~14	6.4	±19	~50	Low-profile VGs are more effective in suppressing the shock-induced separation than passive cavity but also resulted in a higher shock loss.
Mounts and Barber (1992) [19]	Shock-induced separation over flat plate	CFD	$M_\infty = 1.40$	Ramps	0.33	10	6	±14	~50	CFD analysis using 3D Navier–Stokes algorithm indicated low-profile VGs significantly reduce the size of reverse flow region and increase pressure recovery.

Table 2
Summary of vortex characterization research for low-profile VGs

Investigator(s)	Test bed	Type of study	Flow conditions	VG type	h/δ	e/h	β (deg)	Location of crossflow planes examined	Comments
Ashill et al. (2001) [20]; Ashill et al. (2002) [21]	Flat plate	Wind-tunnel test and CFD	$U_\infty = 10$ to 40 m/s, $\delta \sim 60$ mm	Counter-rotating vanes	0.5	~ 10	± 14	Up to $15h$ downstream of VGs [20]; up to $50h$ downstream [21]	A correlation of vortex strength against device Reynolds number has been developed. Spacing between the vanes of counter-rotating VGs reduces the mutual vortex interference. Vortex decay and device drag are reasonably well predicted by a CFD method based on RANS solutions.
				Forward wedge	0.5	10	± 14		
				Backward wedge	0.5	10	± 14		
				Single vane	0.5	10	10, 20, 30, 45		
Yao et al. (2002) [22]	Flat plate	Wind-tunnel Test	$U_\infty = 34$ m/s, $\delta \sim 35$ mm	Single rectangular vane	0.2	7	10, 16, 23	12 stations covering over $100h$ downstream of VG	Detailed flowfield data are obtained for a device-induced embedded streamwise vortex.
Allan et al. (2002) [23]	Flat plate	CFD	$U_\infty = 34$ m/s, $\delta \sim 45$ mm	Single trapezoid vane	0.2	7	10, 23	15, 27, 52, and $102h$ downstream of VG	CFD underestimated the peak vorticity by as much as 40% near the VG.

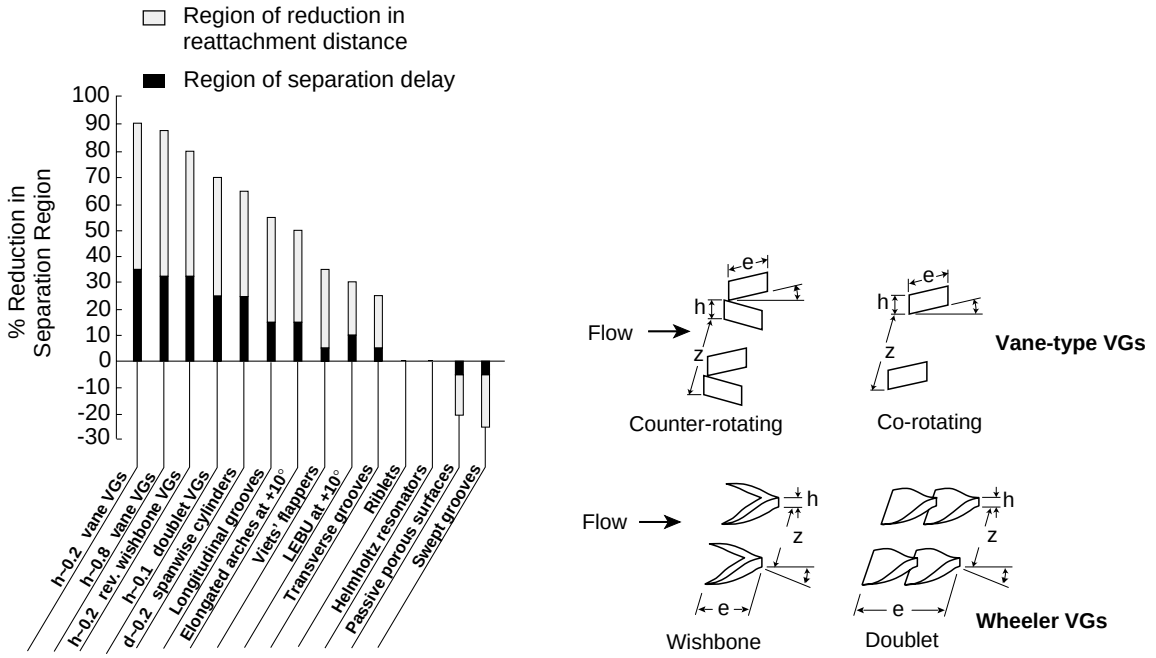

(a) Summary: relative effectiveness in flow separation control versus device category.

(b) VG geometry and device parameters.

Fig. 1. Flow-control effectiveness summary and VG geometry [16].

separation-control effectiveness somewhat; however, the VGs substantially lose their effectiveness when lowering h/δ to less than 0.1. Velocity survey data indicate that a value of $h/\delta < 0.1$ corresponding to $y^+ < 300$, which approximates where the inner (log) region ends and the outer (wake) region begins [16], as illustrated in Fig. 4(a).

The above results demonstrate that for certain applications where the flow-separation line is relatively fixed, the low-profile VGs could be more efficient and effective than the much larger conventional VGs having a device drag an order-of-magnitude higher. The most effective range of low-profile VGs is determined to be about 5–30 h upstream of baseline separation, although the device-induced streamwise vortices could last up to 100 h. Therefore, the low-profile VGs roughly follow many of the same guidelines established by Pearcey [7] for conventional VGs, where the downstream effectiveness, defined as a multiple of h (instead of δ for the conventional VGs), is thereby reduced due to the lower height of the device.

Although both Wheeler's doublet and wishbone VGs could effectively provide flow mixing over 3 times their own device height [15], the performance of low-profile vane-type VGs generally compares favorably with that of the doublet or wishbone VGs. For example, at $h/\delta \sim 0.2$, the vane-type VGs are slightly more effective in separation control while incurring less device drag than the wishbone VGs with equivalent heights. However, the doublet VGs, because of their extended device chord length (double rows), could be more effective than the vane-type VGs when the device height is reduced to only 10% of the boundary-layer thickness [16]. Simplistically, the effectiveness of the low-profile VGs is at least partially attributed to the full velocity-profile characteristic of a turbulent boundary layer. As an example, Fig. 4(b) shows the typical height of low-profile VG relative to the boundary-layer velocity profile. Even at a height of only 0.2δ, the local velocity is over 75% of the free-stream value. Any further increase in height provides only a moderate increase in local velocity but dramatically increases the device drag.

Ashill et al. [20] report a recent experiment performed at the Defence Evaluation and Research Agency (DERA) Boundary Layer Tunnel, Bedford, to examine the comparative effectiveness of flow-separation control over a 2D bump for various low-profile VGs at $U_\infty = 20$ m/s. Wedge type and counter-rotating delta-vane VGs with $h/\delta \sim 0.3$ ($\delta \sim 33$ mm, $e/h \sim 10$, $\Delta z/h = 12$, $\beta = \pm 14^\circ$) are located at $52h$ upstream of the baseline separation. All VG devices examined reduce the extent of the separation region, but the counter-rotating vanes spaced by $1h$ gap are the most effective in this respect. Although the device-induced streamwise

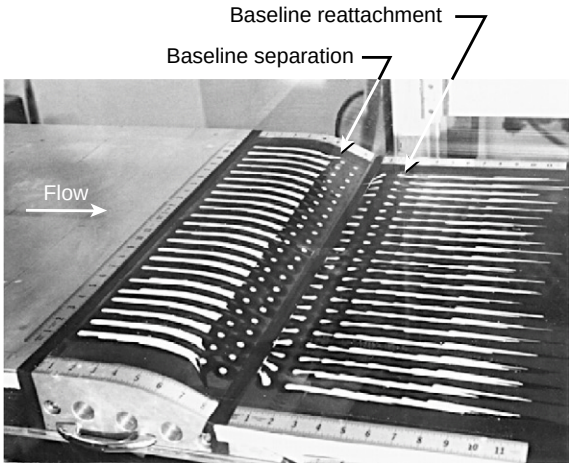

(a) Baseline (VG off) case.

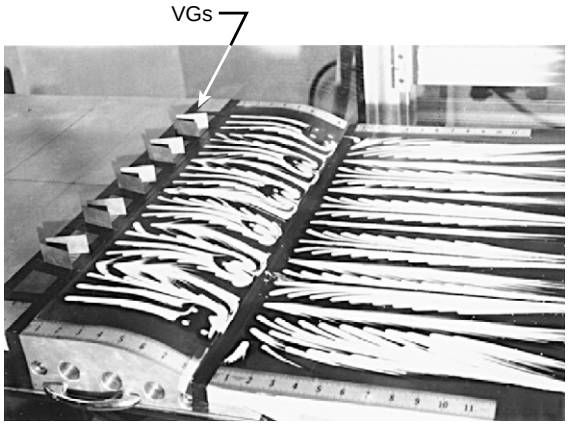

(b) 0.8δ-high vane-type counter-rotating VGs at 6 h upstream of baseline separation.

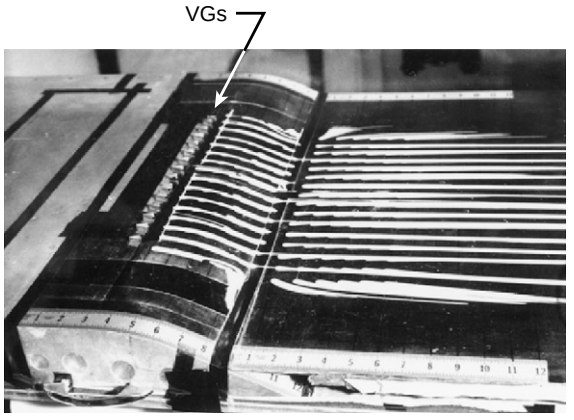

(c) 0.2δ-high vane-type counter-rotating VGs at 10 h upstream of baseline separation.

Fig. 2. Oil-flow visualizations showing the effect of VG on flows over a backward-facing ramp [16].

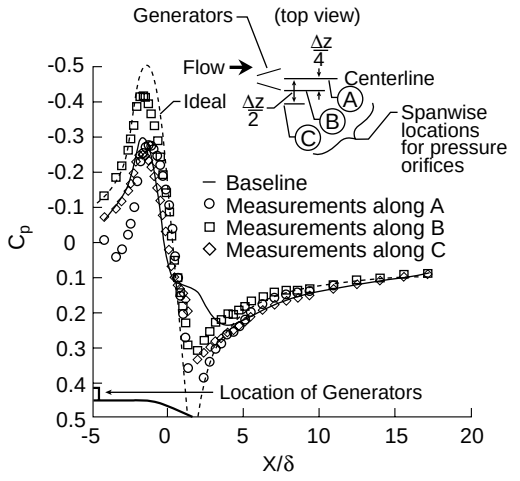

(a) 0.8δ-high vane-type counter-rotating VGs at 6 h upstream of baseline separation.

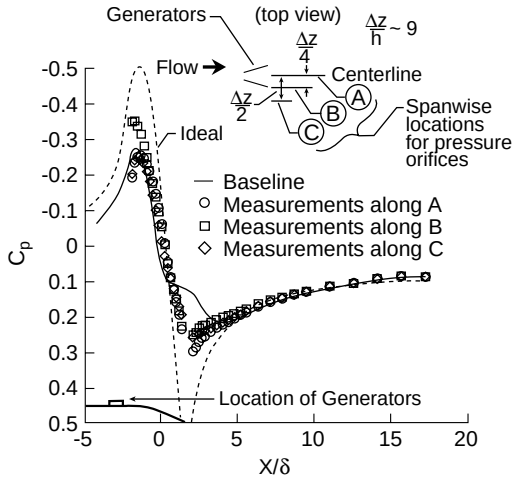

(b) 0.2δ-high vane-type counter-rotating VGs at 10 h upstream of baseline separation.

Fig. 3. Effect of VGs on spanwise variation of the streamwise pressure distributions [16].

vortices are relative weak in the region of separation (after covering 52 h in an adverse pressure gradient), they still maintain the ability to attenuate the separated flow region.

Jenkins et al. [17] present another recent experiment carried out at the NASA Langley Research Center 15-in Low-Turbulence Wind Tunnel at $U_\infty = 140$ ft/s. The flow-control devices are evaluated over a backward-facing ramp that is dominated with 3D separated flow formed by two large juncture vortices—one over each side-corner of the ramp [17]. These two large vortical structures are indicated by the baseline flow-visualization topology shown in Fig. 5(a). The figure highlights two large spiral nodes near the ramp's side edges that

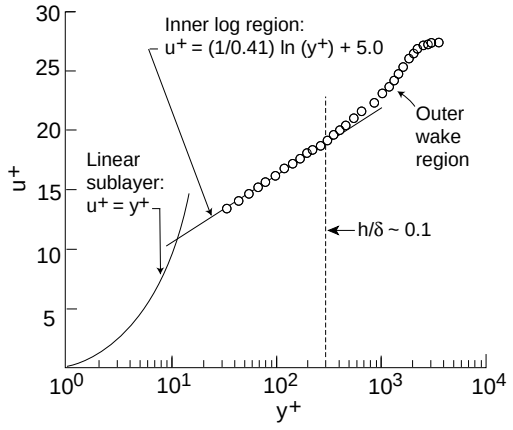

(a) $h/\delta \sim 0.1$ relative to the law of the wall.

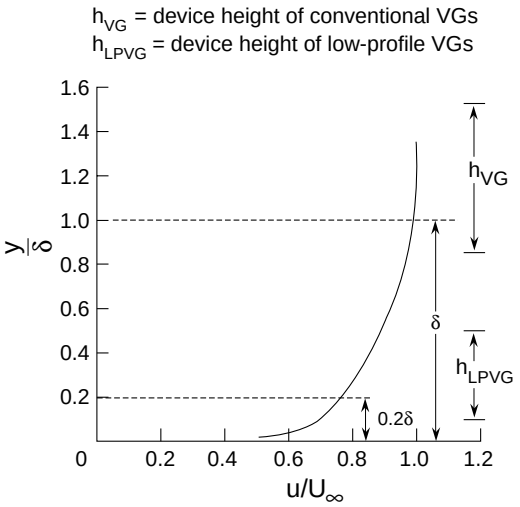

(b) VG height relative to the turbulent boundary-layer velocity profile.

Fig. 4. Low-profile VG height as a function of boundary-layer expressions [16].

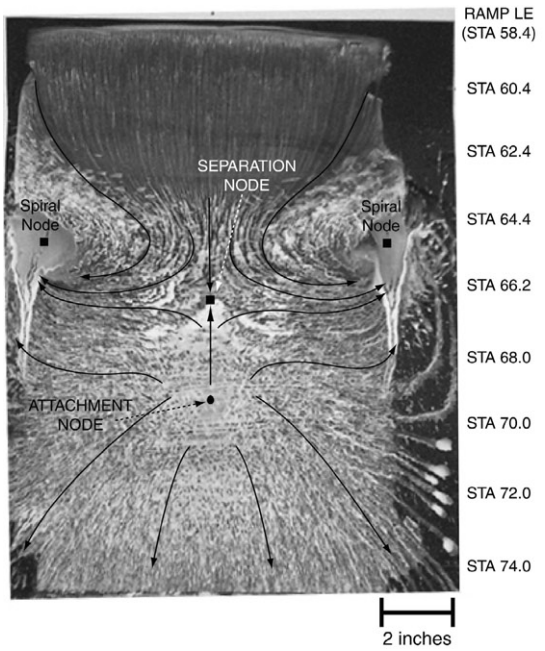

(a) Baseline (VG off) case.

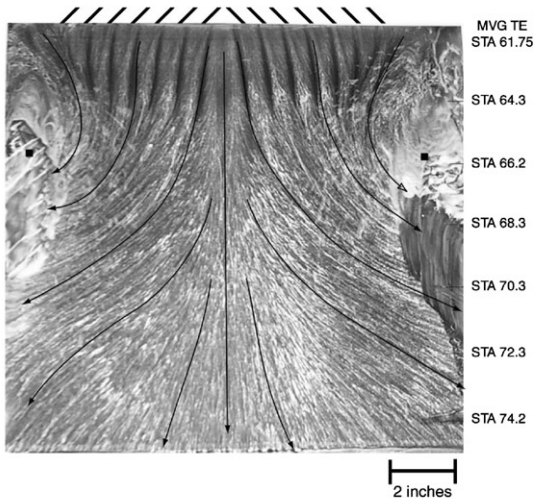

(b) 0.2δ-high vane-type co-rotating VGs at 12 h upstream of baseline separation.

Fig. 5. Oil-flow visualizations showing the effect of VGs on 3D flows over a backward-facing ramp (top view) [17].

reveal the formation of dominate vortical structures and evidence of reverse flow at the center of the ramp.

The co-rotating, trapezoidal-shaped, low-profile VGs (referred to as "micro-vortex generators" by Jenkins et al. [17]) with $h/\delta \sim 0.2\,(e/h = 4,\ \Delta z/h = 4,\ \beta = 23^\circ)$ are highly effective in reducing the 3D flow separation dominated by two large vortical structures, as shown in Fig. 5(b). The oil-flow visualization indicates that an array of embedded miniature streamwise vortices produced by low-profile VGs could redirect the near-wall flows in such a way that the two large vortical structures and associated up-sweep flows are significantly attenuated, allowing the flow in the center of the ramp to remain attached. The effectiveness of generators is confirmed by the surface pressure distributions at the tunnel centerline, as shown in Fig. 6. The "inflection point" in the pressure rise of the baseline distribution corresponds roughly to where the boundary layer separates (station 64). The two low-profile VG cases are observed to effectively control the flow separation through elimination of the inflection point in the pressure distribution and enhancement of the pressure

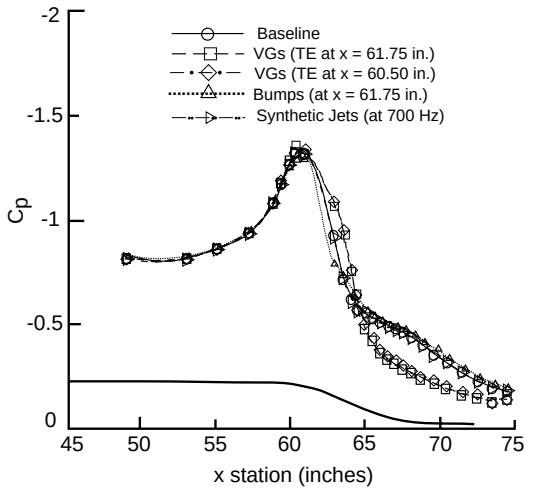

Fig. 6. Comparison of streamwise pressure distributions for low-profile VGs, bumps, and synthetic jets [17].

recovery. The VGs are clearly more effective than other flow-control devices examined, such as the micro bumps and synthetic jets. Results from flowfield measurements using a 3D stereo digital particle image velocimetry (PIV) also indicate much stronger VG-induced streamwise controlling vortices penetrating the near-wall flows [17]. In addition, there is little difference between the VG results at the two locations investigated ($12h$ and $19h$ upstream of baseline separation), which suggests that the device effectiveness is independent of position within at least $20h$ upstream of baseline separation.

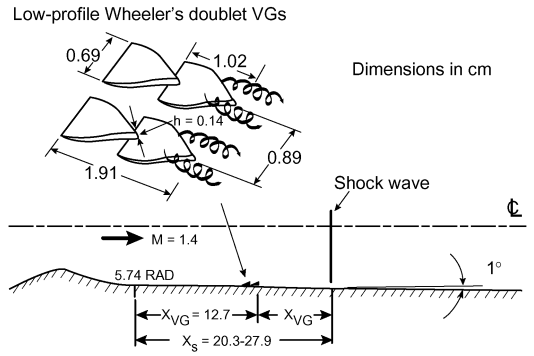

(a) Experimental arrangement for low-profile VGs.

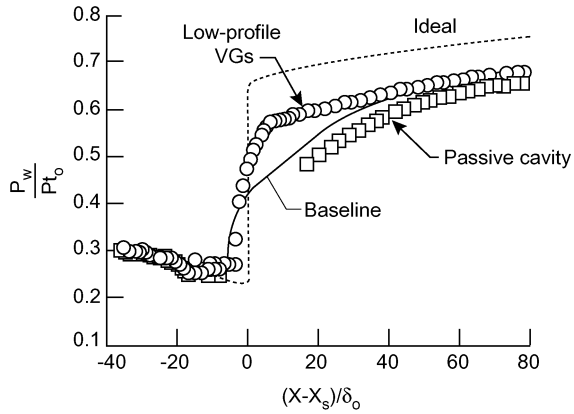

(b) Wall static pressure distributions.

Fig. 7. Shock–boundary layer interaction control using passive devices [18].

2.1.2. Supersonic shock-induced separation

For many aerodynamics applications, such as transonic inlets, diffusers, and airfoils, there is frequently a normal shock interaction with a turbulent boundary layer that has detrimental effects on drag and pressure recovery. McCormick [18] reports a basic experimental study of using low-profile "Wheeler's doublet" VGs [37] to control the shock–boundary layer interaction (Fig. 7(a)). The study shows that the shock strength of Mach 1.56–1.65 was of sufficient magnitude to produce a large separation bubble, thus causing substantial boundary layer losses in an axisymmetric wind tunnel. McCormick [18] chooses the low-profile doublet VGs with $h/\delta \sim 0.36$ ($h = 0.14$ cm, $e/h = 13.6$, $\Delta z/h = 6.4$) for the study because they submerge in the boundary layer and thus disturb the outer supersonic flow less than the conventional VGs, which are typically 1.0–1.2δ in height. The doublet VG arrangement, shown in Fig. 7(a), creates a counter-rotating array of vortices with the second raw of ramps acting like vortex "reinforcers" to enhance the vortex strength without an increase in device height. The VGs are located at approximately $55h$ (20δ) upstream of the shock location.

The performances of low-profile VGs are compared with another flow-control device, the passive cavity, in terms of the wall static pressure distributions, as shown in Fig. 7(b). The "inflection point" in the pressure rise of the baseline distribution (solid line) corresponds roughly to where the boundary layer separates (corresponding to zero on the x-axis). The low-profile VGs (circular symbols) are observed to eliminate the inflection point in the pressure distribution, which indicates that the shock-induced separation is significantly suppressed and thinned [18]. The interaction length (distance from the initial pressure rise to where the distribution parallels the ideal curve) is reduced by a factor of 2.3 from 57 to $25\delta_0$, where δ_0 is the undisturbed boundary-layer thickness at the shock location. The shape of static pressure distribution for the passive cavity (squares in Fig. 7(b)) is very similar to the baseline case but lower in value, and the pressure rise is spread over a larger streamwise (or axial) length. The lower value in static pressure relative to the baseline is partially due to the decrease in

static pressure rise through the more oblique shock system and partially due to the increased thickening of the boundary layer.

McCormick [18] demonstrates that the low-profile VGs significantly suppress the shock-induced separation bubble and improve the boundary-layer characteristics downstream of the shock, as the boundary layer becomes thinner and contains lower mixing losses (lower shape factor). However, suppression of the separation bubble decreases the extent of the low total pressure loss region associated with the lambda foot shock system, which results in a lower mass-averaged total pressure downstream of the shock, as explained in Fig. 8. The figure shows typical surveys of total pressure through the boundary layer at $20\delta_0$ downstream of the shock. The region label "lambda foot benefit" represents the flow from the lambda foot shock system. It is an oblique shock system due to the large boundary-layer displacement caused by separation, which suffers less total pressure loss than a normal shock. The low-profile VG results indicate that the lambda foot benefit farther away from the wall is significantly reduced due to the separation suppression because of higher wall static pressure and healthier boundary-layer shape. In contrast, the passive cavity significantly enhances the extent of the lambda foot benefit region (also see the sketches in Fig. 8). As a result, the passive cavity substantially reduces the total pressure loss through the shock system, and thus wave drag, by causing a more isentropic compression over a larger area. However, the boundary-layer losses downstream of the shock are significantly increased. Thus, the low-profile VGs and passive cavity

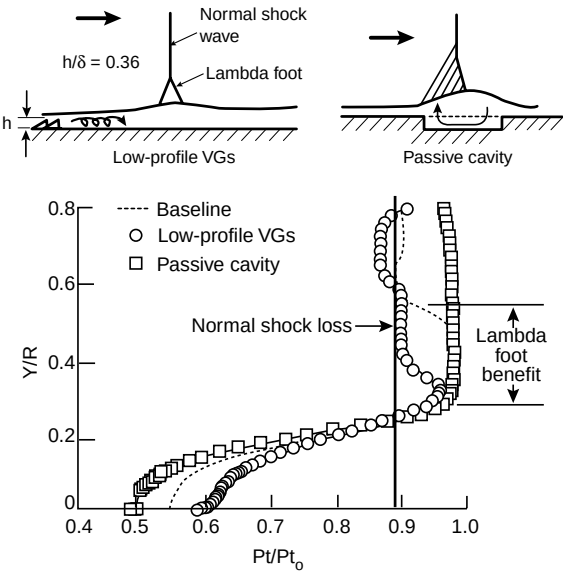

Fig. 8. Effect of shock–boundary layer control on total pressure profiles at $(X-X_s)/\delta_0 = 20$ [18].

offer different advantages and disadvantages, and the preferred approach is application dependent. The low-profile VGs appear to be more applicable for a supersonic diffuser because the shock-induced separation that usually limits diffuser performance is suppressed, allowing more subsonic pressure recovery to be obtained [18]. The increased pressure recovery should more than make up for the increased shock loss; however, if wave drag reduction of an isolated airfoil is required, then the passive cavity is probably more suitable.

Mounts and Barber [19] provide a companion computational fluid dynamics (CFD) analysis of low-profile single ramp VGs with $h/\delta \sim 1/3$ ($e/h = 10$, $\Delta z/h \sim 6$) to alleviate shock-induced separation. The analysis is based on a 3D multiblock, multizone, time-dependent Euler/Navier–Stokes solution algorithm using finite volume discretization. The ramp VGs incorporate into the grid generation at approximately $50\,h$ upstream of the shock location at $M_\infty = 1.40$. Since the analysis is for an unbounded 2D planar case and the VG configurations are different (singular ramp instead of doublet ramps), a direct comparison between the computational results and the experimental data of McCormick [18] is not possible. However, computational analysis supports that the low-profile VGs placed upstream of the shock significantly reduces the size of reverse-flow region (or separation bubble) by up to 45% in the extent and up to 94% in height, which results in sharper rise to pressure recovery. Computational analysis also indicates that it is best to place the VGs at a sufficient distance upstream of shock and thereby allowing the generated streamwise vortices ample time (and distance) to energize the low-momentum boundary-layer flow near the surface.

2.2. Vortex characterization and correlation

Ashill et al. [20,21] present two series of investigations performed at the DERA Boundary Layer Tunnel, Bedford, aimed toward understanding and predicting the flow characteristics of low-profile VGs. Both zero and adverse streamwise pressure gradients are examined at test speeds ranging from 10 to 40 m/s. Various low-profile VGs (referred to as sub boundary-layer vortex generators or SBVGs [20,21]) with $h/\delta \sim 0.5$ ($\delta \sim 60$ mm) are studied and their geometry is shown in Fig. 9(a). The VG geometry consists of counter-rotating vanes, single vane, forwards wedge, and backwards wedge (Schubauer and Spangenber [5] referred to the latter two VGs as "ramp" and "triangular plow", respectively).

Using a laser Doppler anemometer, vortex strength (or circulation, Γ) is determined through flowfield measurements up to $15\,h$ downstream of the device in [20] and up to $50\,h$ downstream in [21]. A framework is suggested in [20] for generalizing the correlation of non-dimensional circulation through using the concept of

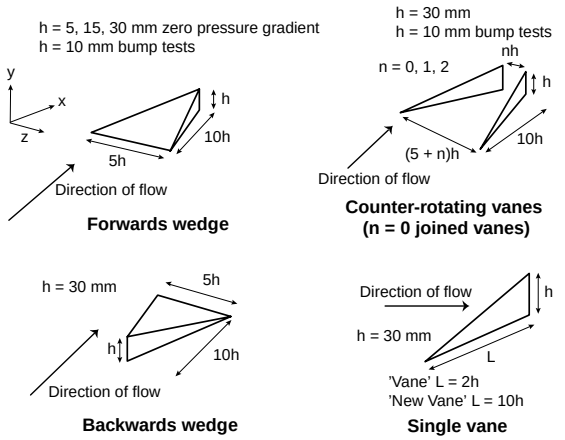

(a) Geometry of SBVGs.

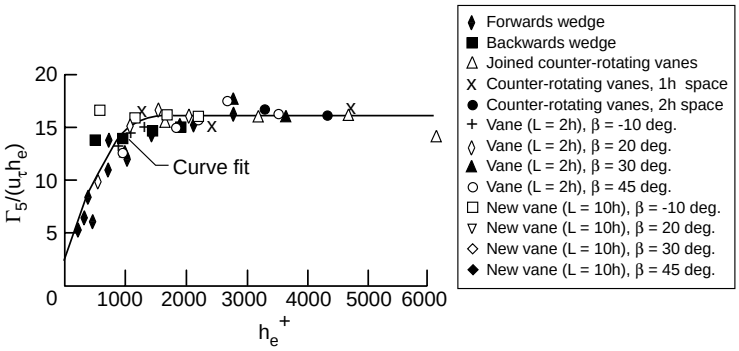

(b) Non-dimensional circulation based on effective height versus non-dimensional effective height.

Fig. 9. Device geometry and correlation of vortex strength against device Reynolds number [20].

a device effective height, h_e [20]. The h_e is selected by ensuring that the maximum value of non-dimensional circulation is independent of device geometry, thereby combining a family of circulation curves for various VGs into a single curve, as shown in Fig. 9(b). The figure shows a single correlation curve of non-dimensional circulation based on effective height, $\Gamma_5/u_\tau h_e$, as a function of non-dimensional effective height, h_e^+ ($h_e^+ = u_\tau h/\nu$), for a location $5h$ downstream of the device trailing edge. The correlation is mostly satisfactory for all VGs examined, even though some points are displaced from the curve that has been fitted through them. Although the effective height does not have any particular relationship with any physical dimension of the devices, the correlation is significant because it enables the predication of vortex strength just downstream of the VGs for a wide range of Reynolds numbers.

The vortex decay within $15h$ downstream of the device in terms of $\ln(\Gamma/\Gamma_{0.5})$ versus non-dimensional streamwise distance, $(x-x_t)/h$ (where x_t is the device trailing edge location), for the counter-rotating VG device with $h/\delta \sim 0.5$ is shown in Fig. 10(a). The suffix 0.5 denotes the Γ value at $0.5h$ downstream of the device. The figure clearly shows that the streamwise decay of vortex strength for the two 1 and $2h$ spaced counter-rotating vane configurations is an order of magnitude lower on a logarithmic basis than that for the forwards wedge, the backwards wedge, and the joined counter-rotating vanes (zero gap ratio, $n = 0h$). Ashill et al. [20] explain that the close proximity of the counter-rotating vortices to one another produced by the forwards wedge and the joint vane device cause mutual interference between the two vortices that leads to additional reduction in vortex strength [20]. The even greater vortex decay of the backwards wedge could be explained by the stronger influence of wall shear in further attenuation of vortex strength because the vortices produced by these devices are always closer to the wall than for the other devices. The decay rates of

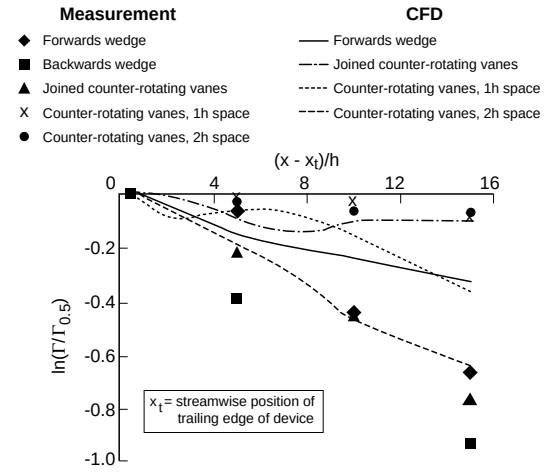

(a) Vortex decay up to 15 h downstream [20].

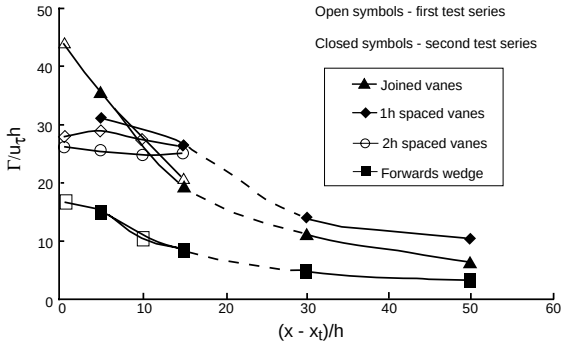

(b) Vortex strength parameter up to 50 h downstream [21].

Fig. 10. Vortex characterization for counter-rotating low-profile VGs with $h/\delta = 0.5$.

the single rotation devices are similar to those of the two counter-rotating devices with spaces, except for the vane at 45° angle of rotation where there is evidence of vortex bursting.

Vortex decay characteristics of forwards wedge, counter-rotating vanes, and a single vane have been established for up to $50h$ downstream of the VG devices [21]. A plot of the vortex strength parameter, $\Gamma/u_\tau h$, as a function of non-dimensional streamwise distance is shown in Fig. 10(b) for all counter-rotating vanes ($n = 0,\ 1,\ 2h$) and the forwards wedge. The vortex strength of the counter-rotating vane is about twice that of the forwards wedge. The vortex decay of both the joined vane and the forwards wedge is clearly larger than that of the spaced vanes ($n = 1,\ 2h$) for a downstream distance of less than $15h$ from the device, as the vortex decay of the spaced vanes in this region is hardly noticeable. Even though the vortex strength of the joined vane is initially larger than that of the spaced vanes at $5h$ or less downstream, the former is lower than the latter at $15h$ or beyond downstream. Thus, the streamwise extent of the effectiveness of the joined vanes is lower than that of spaced vanes.

Ashill et al. [21] report a similar result for an adverse pressure gradient, although to a lesser degree, since adverse pressure gradient tends to promote interaction between the vortices of the spaced vanes. Adverse pressure gradient has less of an effect on vortex decay for a single vane than for counter-rotating vanes. In terms of vortex strength just downstream of the devices, adverse pressure gradient reduces the effectiveness of joined vanes more than for vanes with spaces between them and single vanes. Shape factor results also confirm that the spaced vanes are more effective than the joined vane in adverse pressure gradient [21]. Drag measurements of these low-profile devices based on the wake survey downstream indicate that the forwards wedge has about 40% of the drag of the counter-rotating vanes in zero pressure gradient, which is in agreement with the result of Schubauer and Spangenberg [5] for δ-scale ramps and counter-rotating vanes. Measurements in adverse pressure gradient indicate that increasing the gap ratio (n) of the counter-rotating vanes reduces their device drag.

In addition to the experimental data, Fig. 10(a) also shows CFD predictions of vortex decay for the four counter-rotating VGs described above. The CFD prediction of vortex strength and decay is made by the RANSMB method, which solves the Reynolds-averaged Navier–Stokes (RANS) equations. The $k - g$ turbulence model used is a modification of the Wilcox $k - \omega$ model. The quality of the agreement between CFD and measurement differs from device to device. For some devices, the CFD underestimated the vortex strength just downstream of the device by up to 20%. Vortex decay is reasonably well predicted by CFD within the first $5h$ downstream of the device but the prediction is less satisfactory further downstream. This is probably caused by the difference in computational grid resolutions. The vortex paths of counter-rotating devices are reasonably well predicted by CFD up to $10h$ downstream of the device trailing edge [20]. Device drag of counter-rotating VGs (joined vanes, $1h$ spaced vanes, and forwards wedge) is satisfactorily predicted by CFD in zero pressure gradient [21].

Another recent collaborative investigation involves the detailed flowfield measurements [22] and simulations [23] of an embedded streamwise vortex downstream of a single low-profile vane-type VG placed within a turbulent boundary layer over a flat plate. The studies aim to gain insight and to achieve a more detail evaluation of the reduced CFD model that uses a simplified model of the VG vane, where it eliminates the need to model the device geometry, resulting in a reduced computational cost, as Bender et al. [39] describe. Yao et al. [22] discuss the flowfield

characterization conducted using a 3D stereo digital PIV system in Langley's 20-in × 28-in Shear Flow Tunnel at a free-stream velocity of 34 m/s [22]. The PIV measurements are made at 12 crossflow-plane stations, covering a distance over $100\,h$, downstream of a vane-type VG with $h/\delta \sim 0.20$ ($h = 7$ mm), $e/h = 7$, and three β of 10°, 16° and 23°. The CFD predictions use the NASA OVERFLOW code [40] that solves the compressible RANS equations and uses structured grids in an overset grid framework allowing for the gridding of a complex geometry. Numerical simulations use the two-equation ($k-\omega$) Shear-Stress Transport model of Menter, which performs the best [23]. The flow domain is discretized using five million grid points, including the flow from the leading edge of the flat plate.

Both experimental and CFD results indicate a rapid decay of the peak vorticity downstream of the VG, regardless of the device incidence angle [22,23]. This high rate of vorticity decay might have important flow-control implications, especially for applications associated with an S-duct type of engine inlet where the rapid attenuation of streamwise vortices is highly desirable once the short-range flow-control objective is achieved (also see Section 3.2.2). For the most part, the CFD results agree reasonably well with other aspects of the experiments, such as the predictions of lateral path, vertical path, and circulation. However, the CFD tends to under-predict the strength of peak vorticity and over-predict the vortex size closer to the device (i.e., less than $20\,h$ downstream) by as much as 40% each [22,23]. Hence, there seems to still be a need to improve numerical scheme and/or modeling of turbulence diffusion for the simulation of an embedded streamwise vortex produced by the low-profile VG.

3. Aerodynamics performance enhancement

The applied aerodynamics research for the low-profile VGs also consists of two main categories. The first includes investigations that focused specifically on flow-separation control applications for various airfoils and wings. The second includes those investigations seeking performance improvement through flow control for non-airfoil applications. A chronological summary of representative investigations for each category is presented in Tables 3 and 4. Both Tables 3 and 4 also present summaries of the important device parameters used for flow-separation control (i.e., VG type, h/δ, e/h, $\Delta z/h$, β, and VG placement), similar to those of Tables 1 and 2. The airfoil/wing investigations consist of four sub-categories: low-Reynolds number airfoil, high-lift airfoil, highly swept wings, and transonic airfoil, as shown in Table 3. In-depth discussions of these airfoil/wing applications are presented in Sections 3.1.1–3.1.4, respectively. The non-airfoil investigations include three sub-categories of aircraft interior noise reduction at transonic cruise, engine face flow distortion reduction in compact inlet, and a more efficient overwing fairing (see Table 4). Detailed discussions of these flow-control results are presented, respectively, in Sections 3.2.1–3.2.3. These discussions cover the basic nature of flow separation, the associated performance issues, and the resulting benefits of using the low-profile VGs to control these flow phenomena.

3.1. Airfoil/wing applications

3.1.1. Low-Reynolds number airfoil

Many modern airfoil applications operate in the low-Reynolds number regime, including remotely piloted vehicles, high-altitude aircraft, compressor blades, and wind turbines. Typically, these airfoils operate at a chord Reynolds number of less than one million and often experience a laminar separation bubble for angles of attack below stall. The separation bubble is formed just downstream of the maximum suction pressure where the laminar boundary layer separates and produces an unstable shear layer that rapidly transitions to a reattached turbulent boundary layer where it continues to the airfoil trailing edge. Even though small separation bubbles have little effect upon the lift of an airfoil, they can create a thicker turbulent boundary layer that results in a significant drag increase and thereby adversely affects airfoil efficiency. If the separation bubble can be reduced, a thinner turbulent boundary layer downstream would likely be the result, which could extend the range and endurance of low-Reynolds number aircraft considerably. One of the first applications of the low-profile VGs on an airfoil is for this purpose and was investigated in the early 1990s [24].

Kerho et al. [24] present an experimental investigation conducted at the USC Dryden wind tunnel to reduce the separation bubble on a Liebeck LA2573A low-Reynolds number airfoil through the use of various low-profile VGs (referred to as submerged vortex generators) and thereby reducing the airfoil drag. The chord Reynolds numbers, Re_c, of the airfoil examined are between 2 and 5×10^5 at α below the stall angle, which represent typical operating conditions for a low-Reynolds number airfoil. For controlling the laminar separation bubble, the generators are located immediately downstream of the airfoil's suction pressure peak (at 22% airfoil chord), and are contained completely within the boundary layer. The VGs are intended to produce streamwise vortices that energize the near-wall laminar flow to overcome the adverse pressure gradient, and consequently, suppress the laminar separation bubble and prevent the flowfield from becoming turbulent prematurely. Wishbone VGs [38] with $h/\delta \sim 0.3$ ($\delta \sim 1.6$ mm) and ramp cone VGs with $h/\delta \sim 0.4$ are two different types of low-profile VGs tested, along with a conventional-scale wishbone VGs

Table 3
Summary of research on airfoil/wing aerodynamics performance enhancement using low-profile VGs

Investigator(s)	Test bed	Type of study	Flow parameters	Most effective VG parameters examined						Comments
				VG type	h	e/h	$\Delta z/h$	β (deg)	VG placement	
Low-Reynolds number airfoil:										
Kerho et al. (1993) [24]	Liebeck LA2573A low-Re airfoil	Wind-tunnel test	$Re_c = 20{,}000$ to 500,000, $\delta = 1.6$ mm	Wishbones Ramp cone	0.3δ 0.4δ	10 9	65 40	± 27 60	22% airfoil chord (just up-stream of laminar separation bubble)	0.48-mm-high wishbone VGs can produce a desirable eddy structure without prematurely produce turbulent boundary layer resulting in 38% drag reduction.
High-lift airfoils:										
Lin et al. (1994) [25]; Lin (1999) [16]	3-element high-lift airfoil	Wind-tunnel test	$M_\infty = 0.2$, $Re_c = 5$ and 9×10^6	Counter-rotating trapezoidal vanes	0.2δ	7	13	± 23	25% flap chord (30 h upstream of separation on flap)	0.04-in-high VGs produced 10% lift increase, 50% drag reduction, and 100% increase in L/D. VGs allow stowage inside the flap well during aircraft cruise.
Klausmeyer et al. (1996) [26]	3-element high-lift airfoil	Wind-tunnel test	$U_\infty = 140$ ft/s	Counter-rotating, trapezoidal vanes	0.2δ	7	13	± 23	20% flap chord (27 h upstream of separation on flap)	0.04-in-high VGs produced streamwise vortices strong enough to control separation without dominating the flow field afterward.
Highly swept wings:										
Ashill et al. (1994) [27]; Ashill et al. (1994) [28]; Ashill et al. (1995) [29]; Ashill et al. (1998) [30]	60° LE delta wing model	Wind-tunnel test	$M_\infty = 0.18$, $Re_c = 4 \times 10^6$	Co-rotating wires	$\sim\theta$	45	~ 87	~ 14	50 h from wing LE	0.51-mm-dia. wire VGs provided up to 16% reduction in K and delayed the onset of buffet by 10% in C_L.
Langan and Samuels (1995) [31]	40° LE diamond wing model	Wind-tunnel test	$M_\infty = 0.19$, $Re = 4 \times 10^6$/m $\delta = 0.1$ in	Co-rotating vanes	0.5δ 0.5δ	4 4	12 9	30 10	Wing tip Forward/outboard	0.05-in-high co-rotating VGs provided up to 5% increase in max. L/D.
Transonic airfoil:										
Ashill et al. (2001) [20]	RAE 5243 transonic airfoil	Wind-tunnel test	$M_\infty = 0.67$ to 0.71, $Re_c = 19 \times 10^6$	Counter-rotating vanes Forward wedges	$\sim\delta^*$ $\sim\delta^*$	~ 10 10	12 12	± 14 ± 14	70 h upstream of shock location	0.76-mm-high vanes spaced 1 h apart produced over 20% increase in maximum lift. Forwards wedges increased maximum L/D by 5%.

Table 4
Summary of research on non-airfoil performance enhancement using low-profile VGs

Investigator(s) (year pub.)	Test bed	Type of study	Flow parameters	Most effective VG parameters examined						Comments
				VG type	h	e/h	$\Delta z/h$	β (deg)	VG placement	
Noise reduction for Gulfstream III										
Holmes et al. (1987) [32]	Gulfstream III aircraft	Flight test	$M_\infty = 0.78$ to 0.85, $\delta \sim 1$ in	Counter-rotating rectangular vanes	$1/8\delta$	8	18	± 30	122 in from the aircraft nose (up to about $50h$ up-stream of the shock location)	Up to 5 dB interior noise reduction via delayed shock-induced separation and attenuated Kármán vortex street shed from canopy shock wave.
Engine face distortion management in compact inlets:										
Anabtawi et al. (1999) [33]	Diffusing S-duct	Wind-tunnel test	$M_\infty = 0.05$, $Re_d = 0.5 \times 10^6$	Co-rotating rectangular vanes	0.25δ 0.5δ	10 3	~ 4 ~ 3	~ 16 ~ 16	VG LE at the duct throat	Non-optimum VG placement and small number of device caused the low-profile VGs to be less effective than conventional VGs.
Anderson et al. (1999) [34]	DERA/M2129 inlet S-duct	CFD and DOE	$M_{th} = 0.794$, $Re = 16 \times 10^6$ per feet	Co-rotating rectangular vanes	$\sim \theta$, 2–4 mm	12	~ 12	24	2 throat radius from the inlet	Attenuate large pair of baseline counter-rotating vortices resulting in reduction of DC(60) engine face distortion by over a factor of 3. A reduced CFD model eliminates the need to model the VG geometry.
Hamstra et al. (2000) [35]	4:1 aspect ratio ultra-compact serpentine duct	Wind-tunnel Test	$M_{th} = 0.43$ to 0.68, $Re_d = 3 \times 10^6$	Co-rotating rectangular vanes	$\sim \theta$, 2–3 mm	12	~ 12	24	2 stations down-stream of inlet throat	Up to 5% increase in total pressure recovery. Up to 50% decrease in DC(60) spatial distortion and RMS turbulence.
Overwing fairing of V-22:										
Tai (2002) [36]	V-22 overwing fairing	CFD	$M_\infty = 0.345$	Counter-rotating trapezoidal vanes	0.5δ	3	~ 3	± 9	$\sim 10h$ upstream of baseline separation	New gridding method allows VGs incorporated onto full aircraft for CFD design analysis. Mild separation and marginal benefit predicted for VGs using Baldwin–Lomax turbulence model.

with $h/\delta \sim 0.8$, as shown in the sketch of Fig. 11. A conventional transition (grit) strip comprised of 0.31 mm diameter ($d/\delta \sim 0.2$) glass beads is also tested at the same chord position as the VGs for comparison.

Airfoil drag at the most favorable spacing for each type of generators is shown in Fig. 11, which clearly shows the favorable results obtained through the use of the low-profile VGs. A significant drag reduction is obtained for all three types of VGs at the design condition of $Re_c = 2.35 \times 10^5$ and $\alpha = 4^\circ$. The $h/\delta \sim 0.8$ wishbone VGs ($\Delta z/h \sim 11.3$) produces a 30% drag reduction, the $h/\delta \sim 0.4$ ramped cone VGs ($\Delta z/h \sim 39.7$) yields a 35% drag reduction, and the $h/\delta \sim 0.3$ wishbone VGs ($\Delta z/h \sim 64.6$) provides the best result, a 38% drag reduction [24]. All VGs examined eliminate most of the separation bubble; but the smaller physical heights of the low-profile $h/\delta \sim 0.3$ wishbone and $h/\delta \sim 0.4$ ramp cone VGs provide a smaller profile drag, and their wider spacing also contributes to reducing their device drag more than the larger, $h/\delta \sim 0.8$, wishbone VGs. The figure also shows that the transition strip performs best at a Reynolds number above 3.75×10^5, which corresponds to the optimum bead diameter needed to induce transition. Although a 24% drag reduction is observed at the design conditions of $Re_c = 2.35 \times 10^5$, increasing the bead size to induce transition at a lower Reynolds number would make the bead's performance unacceptable in the mid and upper range of Reynolds numbers. Thus, the VGs appear to provide a much larger range of usefulness [24].

The drag reduction obtained through the use of the VGs is also obvious over a range of lift coefficients (C_L), as shown in the drag polar represented in Fig. 12 at

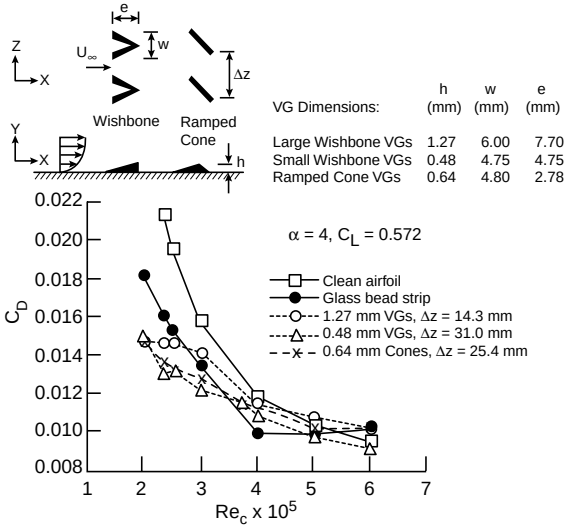

Fig. 11. Drag versus Reynolds number for low-*Re* airfoil with and without laminar flow separation control [24].

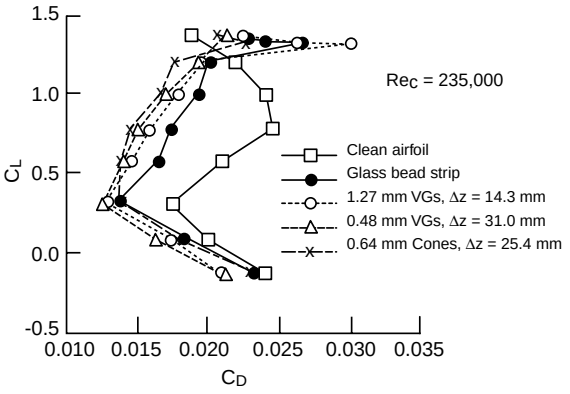

Fig. 12. Lift versus drag at $Re_c = 235,000$ for low-*Re* airfoil with and without laminar flow separation control [24].

$Re_c = 2.35 \times 10^5$. A substantial reduction in airfoil drag by the three types of VGs is seen over the entire midrange of C_L, without any adverse effect (i.e., decrease) on the lift. Particularly, this further illustrates the improved efficiency of the low-profile VGs over the transition strip. The data converge at high C_L near stall because the separation bubble is so small or nonexistent that the VGs have very little effect on the airfoil.

3.1.2. High-lift airfoil

In the process of designing a modern commercial transport aircraft, the performance of its high-lift system is always a critical issue. Flow separation on multi-element high-lift airfoils can be a complicated function of geometry and flight conditions, and can not always be predicted reliably. Previous reports show that certain high-lift configurations exhibit boundary-layer separation on the flap at low angles of attack, while fully attached flap flow occurs near maximum-lift conditions [41,42]. In these cases, altering the geometrical configuration to avoid low angle-of-attack flap separation would have a detrimental effect of reducing the maximum lift. In situations like this, one possible method of maintaining high maximum-lift values while attenuating boundary-layer separation at low angles of attack is to employ flap-mounted, low-profile VGs. The effectiveness of the low-profile VGs in reducing or eliminating separation on a typical single-flap three-element high-lift system at near-flight Reynolds numbers is demonstrated by Lin [16] and Lin et al. [25]. These low-profile VGs, because of their small size, are often referred as "micro-vortex generators" or "micro VGs" [16,25].

The high-lift performance enhancement research using the low-profile VGs is obtained from tests conducted during the early 1990s in the Low-Turbulence Pressure Tunnel at NASA Langley Research Center on a single-flap three-element airfoil [25,41] at $M_\infty = 0.20$

and Re_c of 5 and 9×10^6. These two Reynolds numbers represent typical 3D wind tunnel and flight conditions, respectively, at the critical wing station for low-speed stall of a narrow-body transport. The airfoil has a reference (stowed) airfoil chord, c, of 22 in and the model is configured for landing with a slat deflection of 30° and a flap deflection of 35°. The maximum-lift coefficient, $C_{L,max}$, for this configuration is approximately 4.5 and occurred at $\alpha \sim 21°$. Flow separation occurred on the flap over a broad range of angle of attack ($-4° \leqslant \alpha \leqslant 18°$) below $C_{L,max}$. At a typical landing approach condition ($\alpha \sim 8°$), baseline (VG off) separation on the flap occurs at approximately 45% of the flap chord.

Low-profile, counter-rotating, trapezoid-wing VGs with a height of 0.04 in ($h/c = 0.0018$, $e/h = 7$, $\beta = \pm 23°$) located at 25% of the flap chord (approximately $30h$ upstream of baseline separation) are determined to be the "best-case" configuration. For this case, $h/\delta_{gf} \sim 0.2$, where δ_{gf} is the "local" boundary-layer thickness defined as the distance between the flap surface and the near-wall velocity peak of the gap flow [16,25]. An important practical benefit of this particular placement is that the low-profile VGs are small enough to allow stowage within the flap well during cruise to avoid any device drag penalty when not needed, as illustrated in Fig. 13. The device spacing between each generator pair is rearranged such that the down-wash region is increased and the up-wash region is reduced from the conventional VG design of Taylor [1] to maximize the common downward-flow region to further enhance the wallward momentum transfer for this application.

Separation alleviation on the flap produced by low-profile VGs has a global effect on the flow over the entire high-lift system due to the enhanced "circulation effect", as shown in the surface pressure distributions of Fig. 14 for chord Reynolds number of 9 million. The application of these generators increases the suction pressure on the upper surfaces of the slat and on the main element, in addition to that of the flap. The increase in the suction-pressure levels results in significant lift enhancement at a typical approach angle of attack (i.e., $\alpha = 8°$). For both Reynolds numbers tested, the main element contributes approximately 60% of the increase in lift, while the flap and the slat contributed approximately 25% and 15%, respectively [25]. Just before airfoil stall at $\alpha \sim 21°$, the flow over the flap reattaches, and the generators no longer affect the surface pressure distributions.

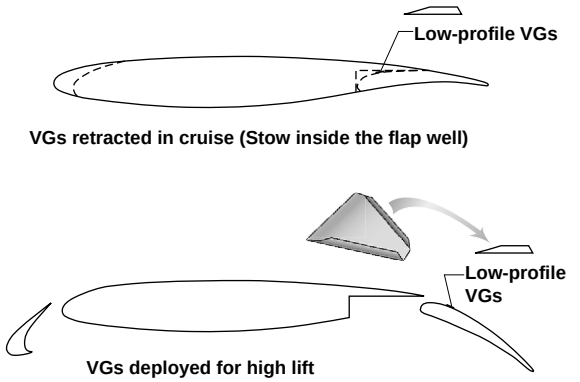

Fig. 13. Cruise and high-lift configurations with the (stowable) trapezoid-wing low-profile VGs [25].

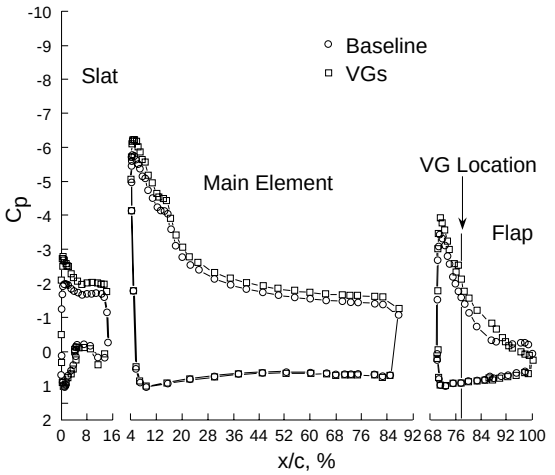

Fig. 14. Effect of low-profile VGs on pressure distributions [25]. ($\alpha = 8°$, $M_\infty = 0.2$, $Re_c = 9 \times 10^6$).

Lift curves and drag polars for the best-case VG configuration with chord Reynolds numbers of 5 and 9 million are shown in Fig. 15, where the $Re_c = 5 \times 10^6$ case has a slightly larger baseline (VG off) separation for $12° \leqslant \alpha \leqslant 16°$. The lift coefficients for the cases of VG-induced attached flow are independent of Reynolds number. The generators do not adversely affect the $C_{L,max}$, where the baseline flow reattaches over the flap. However, the beneficial effects of the VGs on both lift and drag at α below $C_{L,max}$ are dramatic for the high-lift airfoil examined. The large drag reduction with the VG application is a direct result of the significant narrowing of the downstream wake. At typical approach α of 4°–8°, the generator-induced attached flow on the flap could increase the lift on the order of 10%, reduce the drag on the order of 50% (Fig. 15), and increase the lift-to-drag ratio, L/D, on the order of 100% (Fig. 16) [25].

The successful application of low-profile VGs for the high-lift airfoil lead to an interest in obtaining more data on the flowfield affected by these devices. Klausmeyer et al. [26] report on high-lift flowfield measurements conducted at NASA Langley Research Center 2×3-Foot Low-Speed Tunnel on a three-element high-lift airfoil at $U_\infty = 140$ ft/s. A three-component fiber-optic

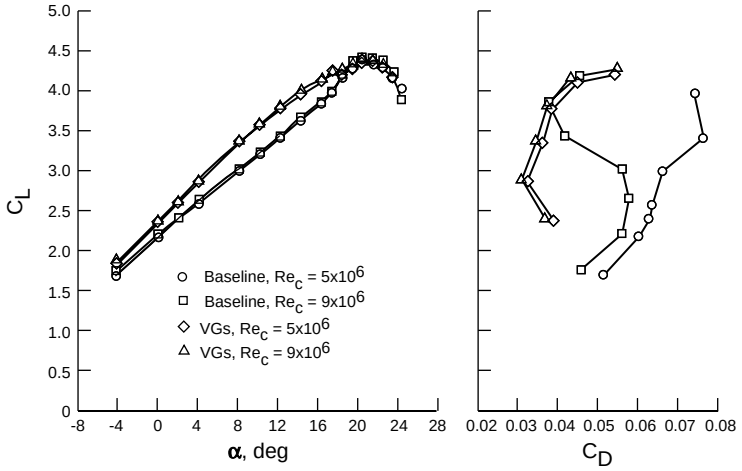

Fig. 15. Effect of low-profile VGs on lift and drag of a high-lift airfoil [25]. ($M_\infty = 0.2$).

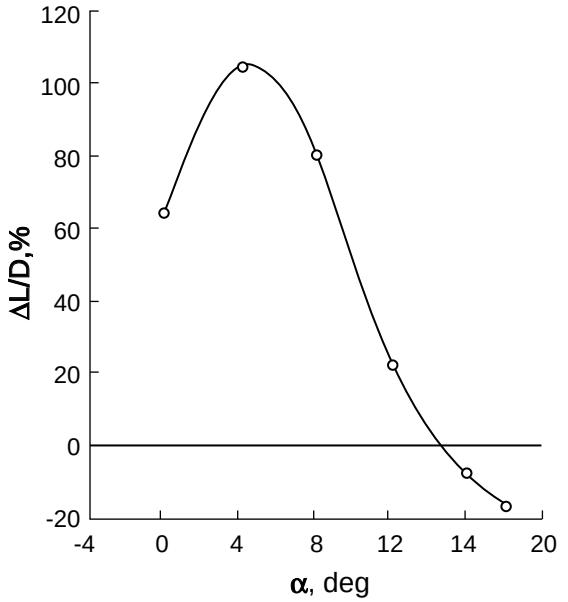

Fig. 16. Effect of low-profile VGs on L/D of a high-lift airfoil [25]. ($M_\infty = 0.2$, $Re_c = 9 \times 10^6$).

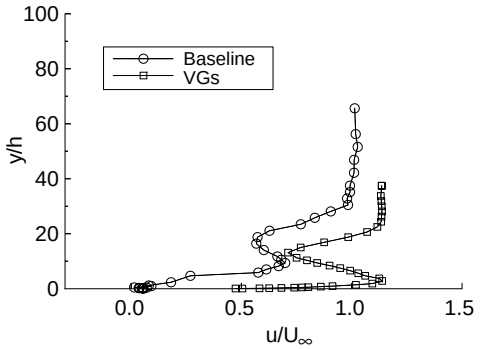

(a) Comparison at mid-flap (50.4% flap chord).

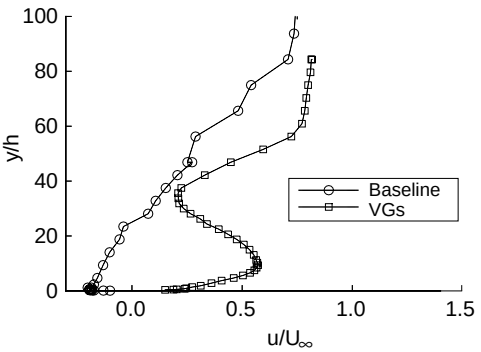

(b) Comparison at flap trailing edge.

Fig. 17. Velocity profiles on flap with and without low-profile VGs [26].

laser Doppler velocimeter system is used to obtain the flowfield measurements. The low-profile VGs used in the study are the same as the counter-rotating trapezoid-wing device Lin et al. [25] describe. The 0.04-in-high VGs ($h/c = 0.0023$) are placed at 20% flap chord. Baseline (VG off) separation on the flap occurs at approximately 40% of the flap chord, and the application of the VGs on the flap causes a complete flow reattachment. Comparisons of mean velocity profiles near mid flap and at the flap trailing edge are shown in Figs. 17(a) and (b), respectively, for the baseline and the VG cases. Fig. 17(a) illustrates a marked thinning of the flap boundary layer due to the generators. Also, higher velocities are obtained outside of the main-element wake due to increased circulation. At the trailing edge

(Fig. 17(b)), the main-element wake is washed out by the recirculation region of the baseline case. The VG case shows a pronounced main-element wake confluent with the flap boundary layer. The significant reduction in velocity defect after flow reattachment would result in a large drag reduction [26].

A plot of peak streamwise (core) vorticity decay is given in Fig. 18. The peak vorticity, $|\omega_x|_{max}$, rapidly attenuated downstream of the generators. The large diffusion of vorticity (or vortex concentration) across core boundaries is probably caused by the steep vorticity gradients between vortex cores as well as the observed secondary vorticity induced by flow shearing between the vortex and the flap surface. In the vicinity of the baseline separation (i.e., 40% flap chord), vortex/boundary-layer interactions may also contribute to further attenuation of vorticity. Fig. 18 illustrates the streamwise distribution of vortex circulation, Γ. The vortex circulation (or strength) drops by a factor of 20 over a distance of approximately 40% of the flap chord [26]. This is a sign of flow-control efficiency, since the low-profile VGs could produce streamwise vortices just strong enough to overcome the baseline separation, yet not so strong such that the streamwise vortices still dominated the boundary layer after the flow attachment is achieved.

3.1.3. Highly swept wings

Ashill et al. [27–30] provide another interesting flow-control application by using miniature wire segments as low-profile VGs (referred as SBVGs) to control the leading-edge flow separation over highly swept wings. Highly swept wings are wings with sweep-back greater than 40° that are suitable for stealthy or supersonic combat or transport aircraft. The research is aimed to reduce the large lift-dependent drag for the highly swept wings so the aircraft could maneuver more efficiently at subsonic speeds. Experiments are performed in the 13 ft × 9 ft Wind Tunnel at DERA, Bedford, on 60° leading-edge delta wing models at a free-stream Mach number of 0.18 and a Reynolds number based on geometric mean chord of 4×10^6.

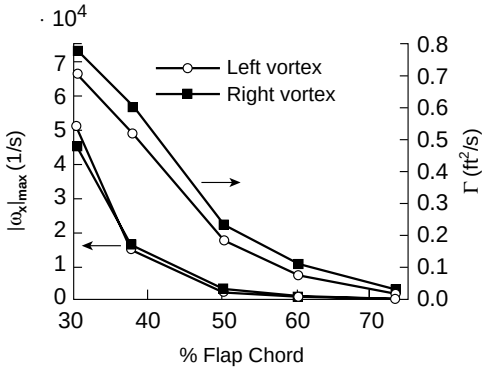

Fig. 18. Streamwise decay of peak vorticity and vortex circulation [26].

Typically in flows over the highly swept wing models, a 3D or "ordinary" separation line, S_1, (described by Kuchemann [43]) occurs on the highly curved part of the upper surface (Fig. 19). In addition, another (unrelated) leading-edge separation line, S_2, occurs downstream of the wing's leading-edge flow-separation point, P. The effect of angle of attack on the streamwise position (x_p) of point P and its consequence are shown in Fig. 19. The figure shows that for α below about 11° (Type A flows), where locally induced separation—S_2 is unaffected by the boundary conditions upstream of P—occurs near the wing tip, the x_p changes only slowly with α. However, at higher α (Type B flows), where the leading-edge separation is upstream dependent (i.e., S_2 depends on the boundary-layer conditions upstream of P), the point P moves more rapidly inboard (and upstream) with increasing α (Fig. 19). Consequently, there is a significant increase in the rate that lift-dependent drag factor, K, increases with α. There is also a noticeable pitch-up at $\alpha \sim 14°$ (Fig. 19). This rapid forward movement of upstream-dependent leading-edge separation with increasing α would have harmful consequences for lateral stability characteristics. Hence the role of the ordinary separation line S_1 is of great significance, and by moving S_1 and P in the downstream direction using the low-profile VGs for the upstream-dependent (Type B) separation may result in significant beneficial effects.

The low-profile VGs investigated are small wires with a diameter, d ($d = 0.51$ mm, $e/d = 45$), approximately equal to the local turbulent boundary layer's displacement thickness, δ^*, and set at an angle of about 16° relative to the wing leading edge (Fig. 20). The wire VGs are tested singly and multiply near the upper wing's leading edge. The detailed location of the wires is specified in Ashill et al. [27–29]. Each wire is arranged so as to induce a streamwise vortex, the rotational sense of which resists the "drift" of the boundary-layer flow toward the point P and to promote the flow toward the separation line deep within the boundary layer. Oil-flow studies indicate that the wires act to convert boundary-layer vorticity into streamwise vorticity. The wire does this by inducing a "scarf" vortex separation upstream of the wire's flat front face. The leeward part of this scarf vortex rolled-up sheet provides the necessary component of streamwise vorticity (Fig. 20). The side of the wire ensures that the windward part of the rolled-up sheet does not interfere with the leeward sheet.

Fig. 21 shows results for the percentage reduction in K due to the wire VGs for the fixed-camber wing plotted against lift coefficient for various numbers and arrangements of wires. The figure shows that the range in which the wire generators are effective is limited to lift

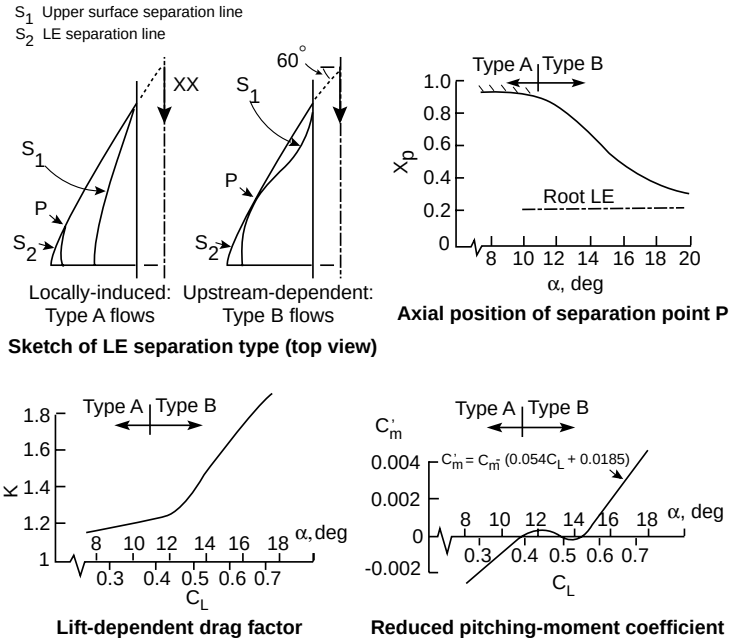

Fig. 19. Leading-edge flows on highly swept wing requiring control [28,29].

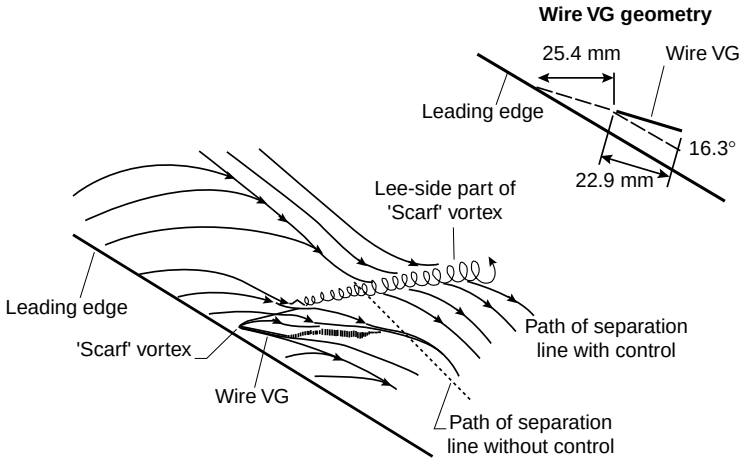

Fig. 20. Surface flows close to a wire VG showing its effect on flow approaching separation line [27].

coefficients between approximately 0.43 and 0.63 ($12^\circ \leqslant \alpha \leqslant 16^\circ$); in addition, the maximum K reduction of 16% occurs with 28 wires at $C_L \sim 0.5$. Any further increase in wire number resulted in a slight decrease in the benefit because of a likely increase in the mutual interference between the wires. Ashill et al. [30] report that studies at DERA indicate a 16% reduction in K can result in significant savings in fleet costs for combat aircraft and reduction in takeoff and landing noise for supersonic transport aircraft.

Ashill et al. [27] indicate that a major part of the increase leading-edge thrust, which provides the reduction in K, comes from the reorganization of the leading-edge separated flow downstream of the point P and moving point P downstream. The wire VGs tighten the leading-edge vortex and move it closer to the forward-facing surface near the wing leading edge, resulting in increased leading-edge thrust. Furthermore, Fig. 22 shows the effect of the wire generators on the wing-tip acceleration for a particular mode of vibration and for

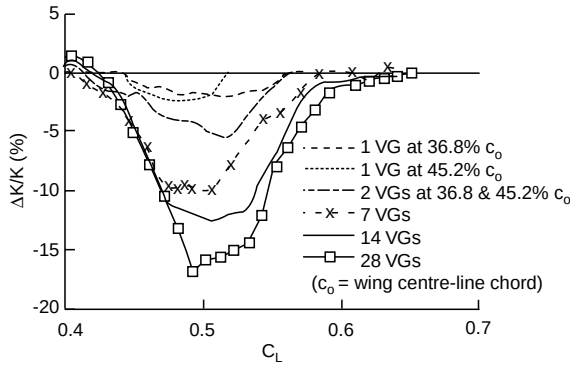

Fig. 21. Effect of wire VGs on lift-dependent drag factor of a highly swept wing [30].

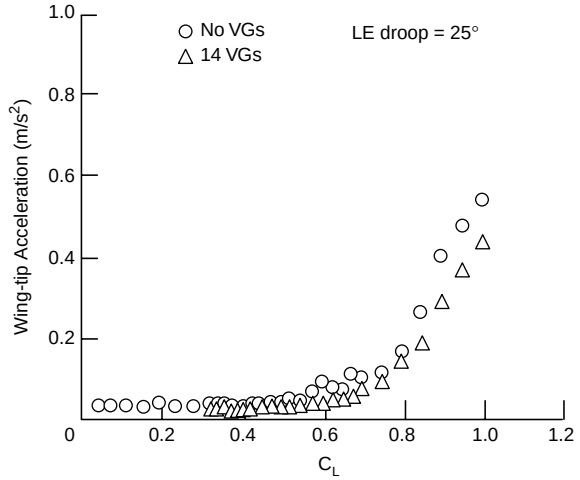

Fig. 22. Effect of wire VGs on wing-tip acceleration of a highly swept wing [30].

a leading-edge droop angle of 25°. It shows that, in addition to reducing K, the low-profile VGs delay the onset of buffet by about 0.05 or almost 10% in lift coefficient, a significant benefit.

A second example of the effect of boundary-layer flow control on swept wings is the maneuver performance enhancement of a modern fighter aircraft. In order to survive in the combat arena, modern and advanced fighter aircraft require the ability to aggressively maneuver in the flight regimes that are characterized by highly separated flowfields, and sometimes strong vortical flows, as reported by Langan and Samuels [31]. These types of flows reduce the effectiveness of conventional aerodynamic controls; the problem is compounded when combining the maneuvering requirement with aircraft geometries designed for low observability.

An investigation is conducted for lift enhancement of a Wright-Patterson Air Force Base fighter aircraft model using various flow-control devices, and among them are the conventional and low-profile VGs [31]. The aircraft model configuration corresponds to a near-term technology, low-observable multirole fighter aircraft with a low-aspect-ratio diamond wing (40° leading-edge and 40° trailing-edge sweeps), a V-tail, and a flow-through inlet on the lower side (Fig. 23). Tests are carried out in the NASA Ames Research Center 7×10-Foot Wind Tunnel at $M_\infty = 0.19$ and $Re = 4 \times 10^6$/m. Baseline flap configuration with a leading-edge/trailing-edge deflection ratio of 20°/0° is selected as the optimum setting because it gives the best maximum L/D (or $L/D_{\max}$) improvement in comparison to the zero flap setting. Parametric variations include the VG geometry, spacing, orientation to the local flow direction, and the location on the wing is shown by the insert-plate position (shaded area) of the aircraft model sketch found in Fig. 23.

Of the VG-configurations investigated, the co-rotating vane-type VGs give the best improvement in terms of maximum L/D [31]. Not surprisingly, the $L/D_{\max}$ improvement of about 6% is obtained for the forward/inboard (FI) location, using conventional VGs with $h/\delta \sim 1$ and a spacing of $\Delta z/h = 9$. But more interestingly, low-profile VGs with $h/\delta \sim 0.5$ are found to be almost as effective in $L/D_{\max}$ enhancement as the conventional generators twice their height (Fig. 21). For example, the $h/\delta \sim 0.5$ VGs located at the wing tip with $\Delta z/h = 12$ and the $h/\delta \sim 0.5$ VGs located at forward/outboard (FO) with $\Delta z/h = 9$ both have the second best $L/D_{\max}$ increase of about 5%. The wishbone VGs [38] with $h/\delta \sim 0.5$, which are rather insensitive to

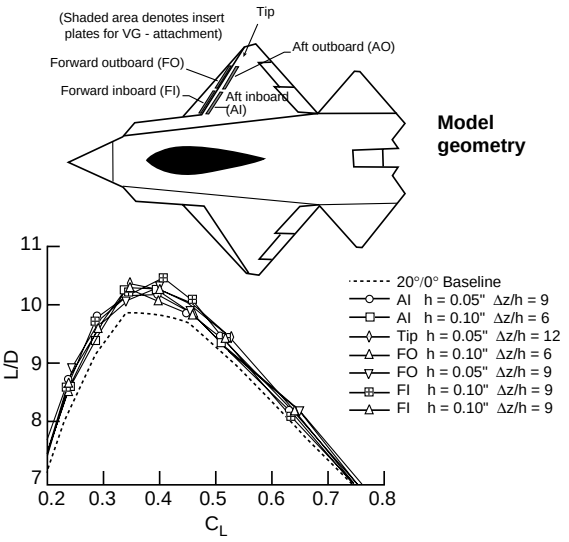

Fig. 23. Effect of co-rotating VGs on L/D of an advanced fighter/attack aircraft model [31].

the local flow direction, produce about the same effectiveness. For this swept-wing application, the counter-rotating vane-type VGs are less effective than those of the co-rotating arrangements in increasing the L/D_{max}. The best-case improvement of counter rotating VGs is about 3.5% [31].

3.1.4. Transonic airfoil

An aircraft needs to generate higher lift coefficients over its wings to achieve the required performance during high-speed turning maneuvers because the vertical component of the lift available to counter the aircraft's weight is substantially reduced. As a result of increased lift requirements, there often can be very large adverse pressure gradients in the streamwise direction as well as shock waves over the wing's upper surface. A possible consequence is that the boundary layer separates, causing a loss of lift and lateral control, high drag, and buffeting [20]. An obvious solution is the use of a low-drag device to control the boundary-layer separation.

Ashill et al. [20] report on tests conducted on a RAE 5243 airfoil model in the 8 ft High-Speed Wind Tunnel at DERA, Bedford, using the low-profile VGs (referred to as SBVGs) for lift enhancement [20]. The airfoil, originally designed for natural laminar flow at a lift coefficient of 0.5 and a Mach number of 0.68, has a chord of 0.635 m and 14% maximum thickness to chord ratio. The shock wave on the upper surface of this airfoil moves only a small distance with changes in Mach number and angle of attack, which is a good candidate for the low-profile VG application, and is located at about 55% chord. The tests are performed for Mach numbers between 0.67 and 0.71 at a Reynolds number based on chord of 19×10^6. The counter-rotating vanes spaced apart by $1\,h$ and forwards wedges are two types of low-profile VGs used for the investigation (Fig. 9(a)). The devices have similar geometry to their counterparts in the low-speed study described in Section 2.2, and the lateral spacing between them is $12\,h$. The VGs has a device height of 0.76 mm or approximately equal to the boundary-layer displacement thickness at the device location (i.e., $h/\delta^* \sim 1$). The generators are placed as an array at 46.5% chord, which is approximately equal to $70\,h$ upstream of the presumed shock location.

Application of low-profile VGs clearly demonstrates a performance improvement in lift. Fig. 24(a) shows normal force coefficient as a function of α for the baseline (uncontrolled) configuration and the two cases with the VGs at a Mach number of 0.71 (i.e., 0.03 Mach higher than the design value). The split vanes give at least 20% higher maximum normal force (or lift) compared with baseline, while the forwards wedges produce about a 10% increase in maximum lift [20]. Fig. 24(b) shows the effect of the generators on L/D. The maximum L/D is obtained with the wedges at a lift

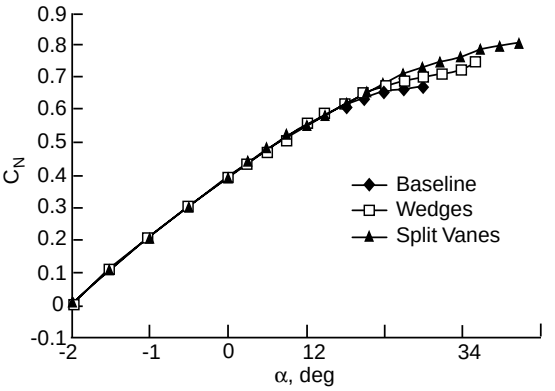

(a) Normal force as a function of airfoil angle of attack.

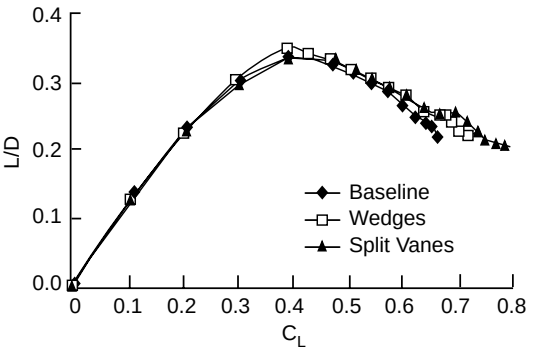

(b) L/D versus lift coefficient.

Fig. 24. Effect of low-profile VGs on lift and drag of a transonic airfoil at $M_\infty = 0.71$ [20].

coefficient of 0.4, which is below that for rapid decrease in pressure near the trailing edge. This is about 5% higher than that of the baseline. The largest values of L/D at lift coefficients above 0.7 are achieved with split vanes, a result that was expected from examining Fig. 24(a)).

The effect of the low-profile VGs on surface pressure distributions at a given lift coefficient of 0.4 is shown in Fig. 25(a). The strength of the shock, indicated by the suction pressure level just upstream of the shock wave, seems to be lowest with the wedges. It is speculated that compression wave induced by wedges, in the presence of the boundary layer, weaken the shock wave. On the other hand, the split vanes produce the largest shock strength, which is possibly a result of the effect of the vanes in reducing the growth of the boundary-layer upstream of the shock (also see discussions in Section 2.1.2). This would result in compression waves of decreased strength in this region [20]. Fig. 25(b) shows that at a lift coefficient of 0.7 (baseline data not available) the split vanes reduce the extent of the separated flow relative to that of the wedges, as expected from viewing Figs. 24(a) and (b).

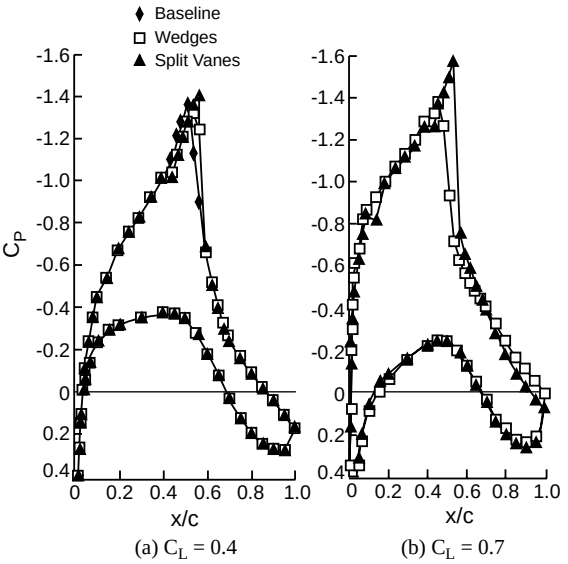

(a) $C_L = 0.4$ (b) $C_L = 0.7$

Fig. 25. Effect of low-profile VGs on pressure distributions of a transonic airfoil at $M_\infty = 0.71$ [20].

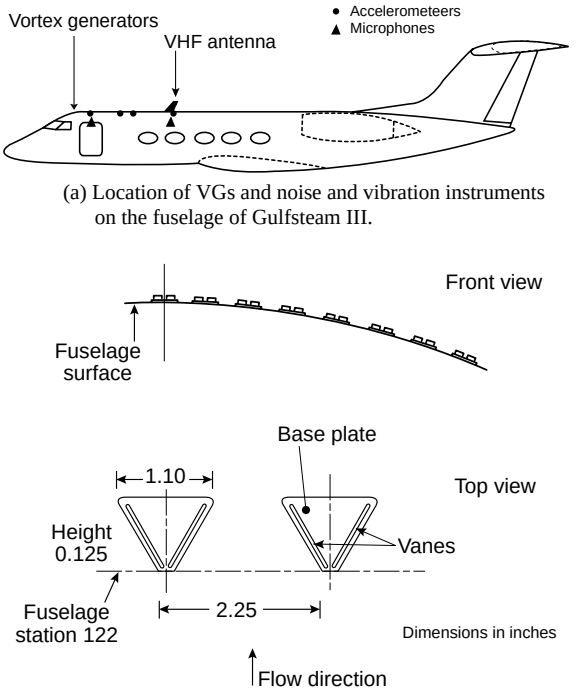

(a) Location of VGs and noise and vibration instruments on the fuselage of Gulfsteam III.

(b) Geometry of low-profile VGs on the aircraft fuselage.

Fig. 26. Low-profile VGs for interior noise reduction on a Gulfstream III flight-test aircraft [32].

3.2. Non-airfoil applications

3.2.1. Noise reduction for Gulfstream III

One of the earliest practical applications of the low-profile VGs is not intended for an airfoil or wing, but instead, it is for interior noise reduction of the Gulfstream III aircraft [32]. From research in the mid-1980s, it is discovered that a small region of shock-induced boundary-layer flow separation exists at high Mach numbers on the canopy of the Gulfstream III aircraft (Fig. 26(a)). Downstream of the separated flow region an externally mounted VHF blade antenna generates a vibration with a frequency spike at 240 Hz. This vibration appears to be produced by an unsteady vortex separation that might be excited by a von Kármán vortex street shed from the canopy shock wave. As a result, a low-frequency noise known as "Mach rumble" is observed in the cabin of the Gulfstream III aircraft at high Mach number cruise conditions, and the interior noise tends to intensify with an increase in Mach number [32].

Inspired by the work of Kuethe [11], in which wave-type low-profile VGs are successful in suppressing the formation of the Kármán vortex street in the wake region, Holmes et al. [32] select low-profile, 1/8-in-high VGs (referred as SBVGs) for this flow-control application. Furthermore, the local flow over the canopy being supersonic also indicates that conventional VGs would create stronger shocks and hence additional noise sources, whereas the low-profile VGs function in the lower portion of the boundary layer in a subsonic flow region. The selected device height is about 1/8 of the predicted boundary-layer thickness ($\delta \sim 1$ in). The small device height also means associated device drag and aesthetic impacts are minimized [32]. As discussed earlier in Section 2.1.1, their small size means that the low-profile VGs have a somewhat limited range of downstream effectiveness. Hence, placement of these VGs relative to the shock wave becomes more critical than it would be for the conventional VGs. The geometry of the low-profile VGs examined is shown in Fig. 26(b), which consists of a row of counter-rotating vane pair with $e/h = 8$, $\Delta z/h = 18$, and $\beta = \pm 30^\circ$. Both e/h and $\Delta z/h$ are about a factor of 4 higher and β is 14° higher than the classical design guideline for the conventional VGs. This combination of a relative longer vane chord, wider spacing, and higher incidence angle ensure the generation of strong embedded streamwise vortices as well as reduce the overall number of devices required for the application (lower device drag). See Fig. 26 for device location and geometry. Fig. 26(a) also shows the placement of noise and vibration instruments at six centerline locations inside the fuselage of a Gulfstream III flight-test aircraft.

Installing a number of low-profile VGs to the fuselage upstream of the shock very effectively reduces both the Mach rumble and the vibration. Acting much like the conventional VGs, the low-profile VGs effectively delay

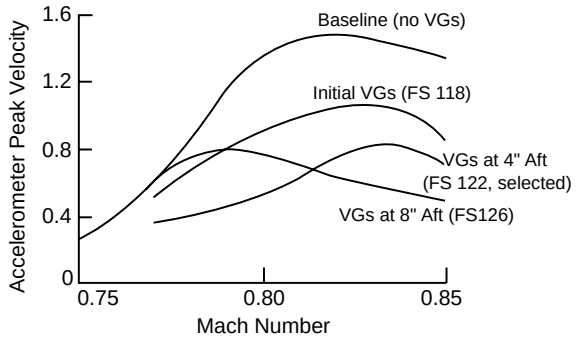

Fig. 27. Effect of device streamwise location on vibration [32].

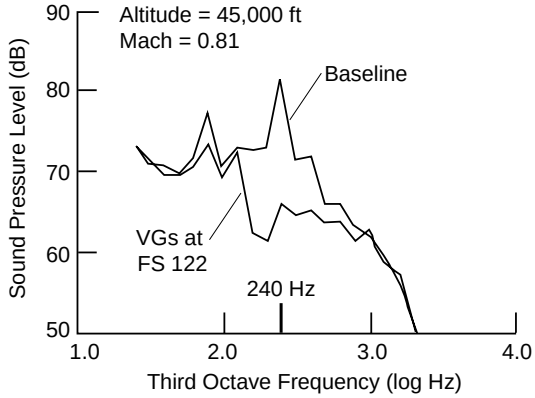

(a) Interior acoustic spectra.

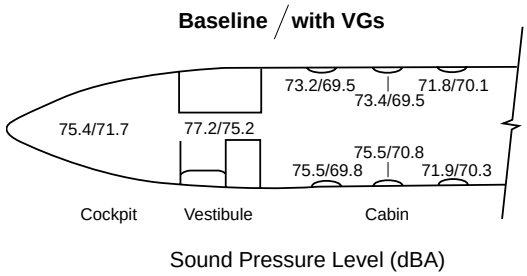

(b) Interior acoustic survey.

Fig. 28. Effect of low-profile VGs on acoustic measurements [32].

separation as well as break up the Kármán vortex street, eliminating two major noise sources [32]. Flight test results of the test variable at the forward accelerometer position (vestibule area) are presented in Fig. 27, along with the untreated canopy (baseline) test results. As expected, the accelerometer data indicate an increase in the baseline shock strength and aft movement of the shock with increase in Mach number. The initial VG location of fuselage station FS118 (or 118 in from the nose) is selected based on computational analysis. The finite downstream effectiveness of the device requires a location close to the aft higher-strength shock at Mach 0.85. However, the aft most position (FS126) is too far aft to be properly positioned to control the more forward shock position at lower Mach number. As a design trade off, a position just 4 in aft the initial location (FS122) is selected for the final VG configuration. The final configuration of 15 generator pairs perform best overall in significantly reducing the severity of separation induced by the fuselage shock for a range of flight Mach numbers from about 0.78 to more than 0.85.

The flight test results, in terms of third-octave frequency spectra, are shown in Fig. 28(a) at a forward cabin seat location. The blade antenna clearly no longer produce a strong vibration spike at 240 Hz, a result attributed to a marked reduction in the flow turbulence exciting the vibration. Acoustic measurement results throughout the cabin are summarized in Fig. 28(b), in terms of A-weighted sound level (dBA), for a selected cruise condition. A substantial cabin noise reduction of up to approximately 5 dBA is achieved [32].

3.2.2. Engine face distortion management in compact inlet

The current development strategy for combat aircraft is directed toward reduction in the Life-Cycle Cost with little or no compromise to the vehicle performance and survivability. This strategy is extended to the aircraft component level, in particular, the engine inlet system. One method to reduce inlet system Life-Cycle Cost is to reduce its structural weight and volume. Consequently, advanced S-duct inlet configurations are being made more compact (or shorter) to achieve weight and volume (and cost) reduction. However, the compact S-ducts are characterized by high distortion and low pressure recovery produced by extreme wall curvature and strong secondary flow gradients. Therefore, in order to achieve acceptable performance levels in such advanced compact inlet configurations, flow-control methods are required to manage their flowfield [33–35].

The use of conventional VGs to control inlet flow distortion and thereby achieve global secondary flow control downstream is first proposed and subsequently established by Anderson et al. [44,45]. During the late 1990s, Anabtawi et al. [33] experimentally use the low-profile VGs with $h/\delta \sim 0.25$ and 0.5 and conventional VGs with $h/\delta \sim 1$ to lower the total pressure distortion within the diffusing S-duct. Although the low-profile VGs could lower the level of converted equivalent values of DC(60) at $M = 0.85$ from 14% of the baseline to 9.1% for $h/\delta \sim 0.25$ VGs and 7.2% for $h/\delta \sim 0.5$ VGs, they are not quite as good as the 3.4% achieved for the $h/\delta \sim 1$ VGs. Anabtawi et al. [33] cite that the non-optimum localized placement of generators (relative to

flow separation) and the small number of devices used may be the reason for the ineffectiveness of the smaller VGs. Placing the low-profile VGs inside and around the surface of the duct closer to region of separation in an attempt to evenly redistribute the boundary-layer flow around the circumference of the fan face is suggested as an improvement [33].

At about the same time, Anderson et al. [34] use CFD and design of experiment (DOE) optimization procedures to examine the effect of using low-profile co-rotating vane VGs to "globally" manage the entire inlet flowfield. The DOE method [46] is applied in the form of a predetermined design array that defines a series of experiments that can evaluate the effects of each design variable over its range of values. The low-profile VGs with a device height on the order of boundary-layer momentum thickness, θ, are found to effectively spread out (circumferentially) the near-wall low-momentum fluids that suppress 3D flow separation from the wall. The research is done as a necessary prerequisite to define the controlling properties for the future applications of micro electrical mechanical systems (MEMS) actuators. These actuators share the same objective of effectively managing the entire flowfield of compact inlets using the similar approach of "minimal" near-wall protuberances as the low-profile VGs, hence the VG vanes Anderson et al. [34] used are called the MEMS-scale effectors.

The CFD investigations are conducted on the DERA/M2129 inlet S-duct at $M_{th}, = 0.8$ and $Re = 16 \times 10^6$/ft, using the Lockheed Martin Tactical Aircraft Systems' Full Navier-Stokes FALCON code [39] that includes a vane VG (effector) model. Two types of gridding methods are used for comparison: the effector analysis grid and the effector model grid. The difference between the two methods is that the individual vanes were not gridded for the effector model grid. The latter uses a simplified model of the VG vane by the means of the boundary condition approach rather than fully gridding the VGs. As a result, the effector model grid contains 539,700 fewer nodal points (72% less) than the effector analysis grid and requires less computational cost [34].

The reference effector installation is defined as a VG configuration such that the vane height is between 2 and 4 mm above the duct walls, or $h \sim \theta$. Fig. 29(a) illustrates the Full Navier–Stokes baseline solution for the 3D flow-separation topography associated with vortex lift-off in the M2129 inlet S-duct. The figure shows the development of a pair of counter-rotating vortices that form in the forward section of the duct, which leads to vortex lift-off in the aft section. It is this lift-off or 3D separation phenomenon that is the primary distortion mechanism in compact inlet systems, and thereby the flow phenomena that must be controlled. The purpose of the low-profile co-rotating VGs is to create vortices that merge quickly to form a single overall secondary flow pattern that remains within the "thin" boundary layer next to the wall. It is this induced secondary flow pattern adjacent to the wall that prevents the formation of the pair of counter-rotating vortices described in Fig. 29(a), and consequently the undesirable effects of the vortex lift-off phenomena on engine face flow distortion. Producing this single overall secondary flow pattern is the fundamental flow mechanism that allows the entire inlet flowfield to be managed by controlling (or redistributing) the flow within a thin layer adjacent to the walls, as reported by Anderson et al. [34].

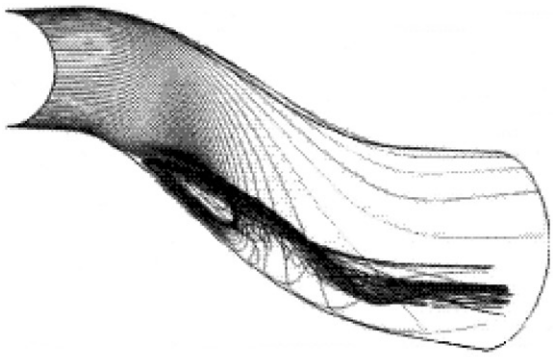

(a) Particle traces showing the 3D vortex separation within the baseline (M2129) inlet S-duct.

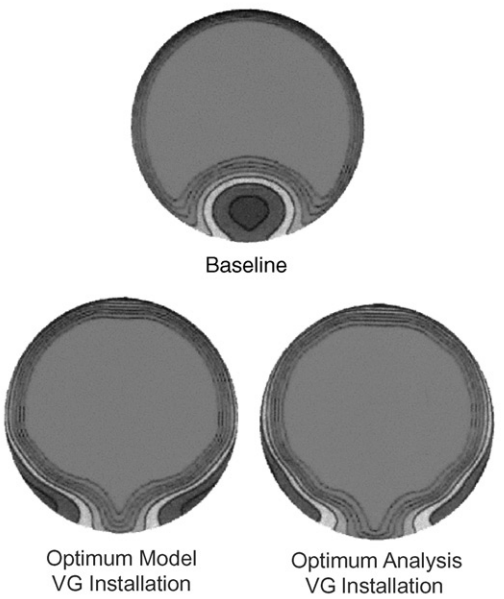

(b) Engine face total pressure recovery contours.

Fig. 29. Effect of low-profiles VGs in a compact (M2129) inlet S-duct [34].

The baseline engine face total pressure recovery contours obtained from the FFA/Sweden T1500 High

Reynolds Number Wind Tunnel are shown in Fig. 29(b). The engine face flow distortion caused by the pair of counter-rotating vortices described in Fig. 29(a) are clearly seen in the pressure contours. Based on results using CFD and DOE optimization procedures, it is concluded that the performance of the low-profile VGs is very sensitive to the device arrangement (design). There appears to be an optimum number of VGs that can be installed in any installation band, and this value is 36 for optimal analysis and 34 for optimal model. Beyond that optimum number, the reduction in engine face DC(60) distortion is negligible. In any installation arrangement, there is an optimum strength directly associated with device angle of incidence (β) and the values of β are 24° and 28°, respectively, for optimal analysis and optimal model. The optimum device strength does not depend strongly on the number of device within the installation itself. The device chord length is found to be a very effective parameter in reducing engine face flow distortion, and the device chord length non-dimensionalized by throat radius is 0.168 for both optimal analysis and optimal model [34].

A comparison of the total pressure recovery contours using optimal analysis and optimal model methods is shown in Fig. 29(b). There is dramatic improvement over the baseline, although little difference appears both qualitatively and quantitatively between the two computational methods. Of course, the optimal model method has the advantage of using 72% less nodal points. As the large pair of counter-rotating vortices is eliminated from the bottom duct surface of the baseline case, the DC(60) engine face distortion is predicted to reduce by a factor of 3.5, from 0.336 to 0.096 using the most conservative results of the optimum analysis method.

A subsequent experimental verification test conducted at the W1B Subsonic Diffuser Test Facility at NASA Glenn Research Center examines the effect of low-profile VGs on a 4:1 aspect ratio ultra-compact (length/diameter = 2.5) serpentine duct that fully obscures line-of-sight view of the engine face [35]. The throat Mach number for the test ranges from 0.43 to 0.68, and the Reynolds number based on "aerodynamic interface plane" diameter, Re_d, is approximately 3×10^6. Two arrays of 36 co-rotating low-profile VGs (referred to as microvanes by Hamstra et al. [35]) with device height ranging from 2 to 3 mm are used.

Substantial improvements in all inlet system-level metrics are found for the low-profile VGs across the tested range. A comparison of pressure recovery, distortion, and RMS turbulent levels for the baseline, low-profile VG, and a microjet configuration is shown in Fig. 30. The low-profile VGs provide dramatic improvement over the baseline and microjet configurations in both pressure recovery and turbulence over the entire test range, and in distortion up to a throat Mach number of 0.60. In particular, total pressure recovery is increased by as much as 5%, and DC(60) spatial distortion and RMS turbulence are decreased by as much as 50% [35]. CFD predictions compare very well with experimental data for substantial performance improvement through the application of low-profile VGs.

3.2.3. *Overwing fairing of V-22*

Tai [36] of the Naval Surface Warfare Center—Carderock Division researches CFD using a multizone thin-layer Navier–Stokes method to evaluate the effectiveness of low-profile VGs (referred to as micro-vortex generators). These VGs are simulated on the overwing fairing of V-22 aircraft to enhance its forward-flight aerodynamics performance. Computational analysis uses NASA Langley's CFL3D code [47] (with modifications for applying specific boundary conditions) as the flow solver for a structured grid. A new gridding procedure developed uses NASA Ames 3DGRAPE code [48] for both master (basic) and sub-region grid generations, as well as the CNS/ZONER code [49] for zoning and clustering. The procedure involves creation of six-sided "holes" within the master grid of the aircraft and the six faces of each hole are used as the boundaries for generating the sub-region grid that contains each VG. This process allows for the seamless embedding of the VGs (sub-region grid) onto the modeling of the aircraft (master grid) without mesh over-lapping at each boundary [36]. Because of its relatively small sub-boundary-layer size, if the VGs are embedded using the Chimera type scheme, the resulting effect could be swallowed by inaccuracies due to grid overlapping and interpolations.

Ten VGs are simulated on a modified overwing fairing of the V-22 aircraft. The generators used are vane-type counter-rotating trapezoid-wing shaped with $h = 2.0$ in ($e/h = 3$, $\Delta z/h \sim 3$). Using a modified Baldwin–Lomax turbulence model, the computed total velocity vectors above the surface of the overwing fairing and particle traces over the entire aircraft are plotted for the design cruise angles of attack of 7°, for configurations with and without the VGs. Fig. 31(a) shows the velocity vectors and particle traces of baseline (Configuration A) where the flow is mostly attached on the fairing except at the trailing edge, indicating that the need for using the VG is there, but not crucial. Computational results indicate that separation enhancement could be an undesirable result if the generators are too large or improperly placed too far forward of the baseline separation, as in the case of Configuration B (Fig. 31(b)). The figure shows that the flow begins to separate at mid chord and the separation region extends well beyond the trailing edge. However, by moving the generators closer to approximately $10h$ upstream of the baseline (mild) separation and reducing the device incidence angle (β)

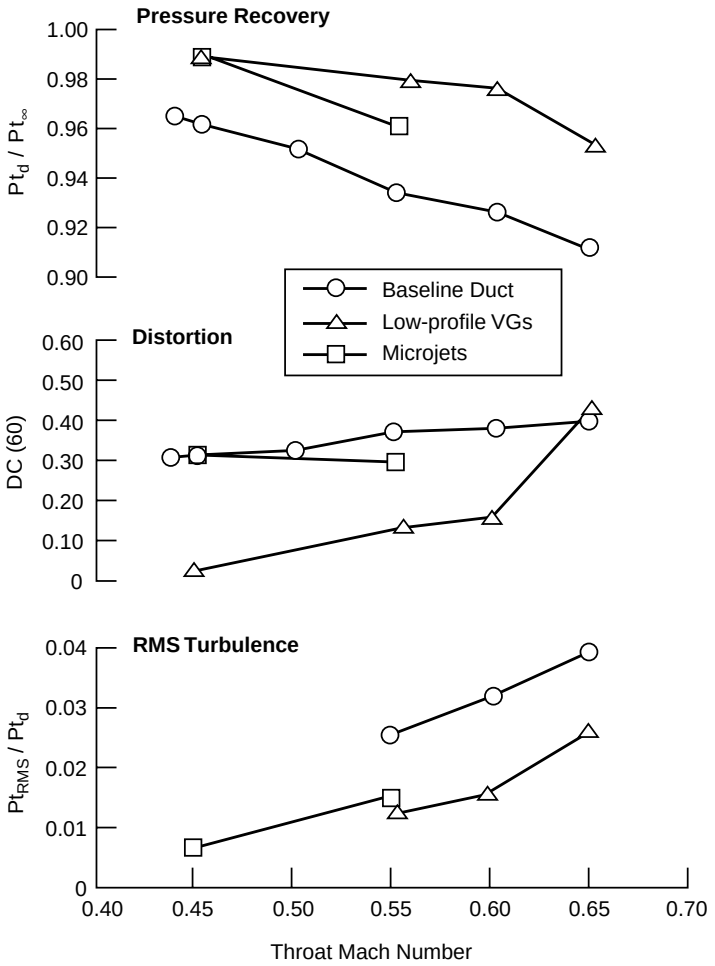

Fig. 30. Performance enhancement metrics for low-profile VGs and microjet configurations [35].

from $\pm 20^\circ$ to $\pm 9^\circ$, this new configuration completely eliminates the flow separation (Configuration E), as shown in Fig. 31(c). The above trends persist as the aircraft α increased to 10° [36]. Upon a closer examination of the velocity profile data, the h/δ for Configuration E (best case) is found to be about 0.5, which makes the generators low-profile VGs; whereas for Configuration B, the h/δ is on the order of 1, which makes them the conventional VGs.

The CFD results using the Baldwin–Lomax model are for the most part agreed with the more sophisticated Menter κ-ω model. However, the Menter model yields less tendency for flow separation; consequently there is no evidence of separation in the baseline case and therefore no performance improvements are predicted for the VG applications. Using the Baldwin–Lomax model for the best-case flow-control application (Configuration E), the L/D improvements for the whole aircraft are 0.4% and 1% for 7° and 10° angle of attack, respectively [36]. These performance improvements are relatively small and subject to verification by further wind tunnel or flight tests. In addition, there is reason to believe that the modified Baldwin–Lomax model may have "over-predicted" the flow separation in these vortex dominated flows that include baseline and Configuration B. Of course, if there is no flow separation for the baseline aircraft configuration, then there is no need to use VGs for flow control. Nevertheless, the study did clearly demonstrate an important point: that it is "possible" to incorporate the low-profile VGs for CFD design, with substantial detail and fidelity, through innovated gridding for a complex aircraft configuration such as the V-22. Further refinements to this technique are to be expected.

4. Concluding remarks

This paper reviews and highlights several research efforts on boundary-layer flow-separation control using

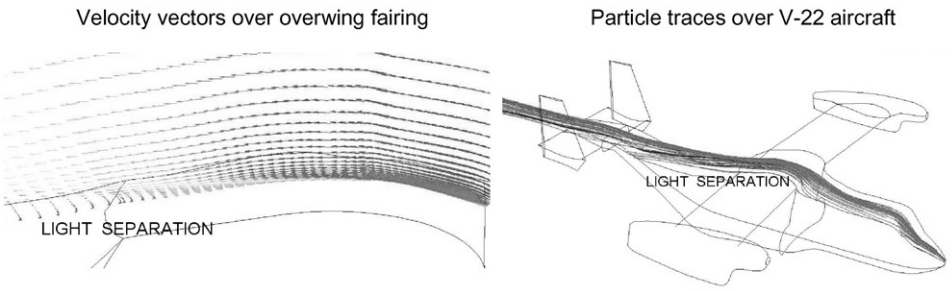

(a) VG off baseline (Configuration A).

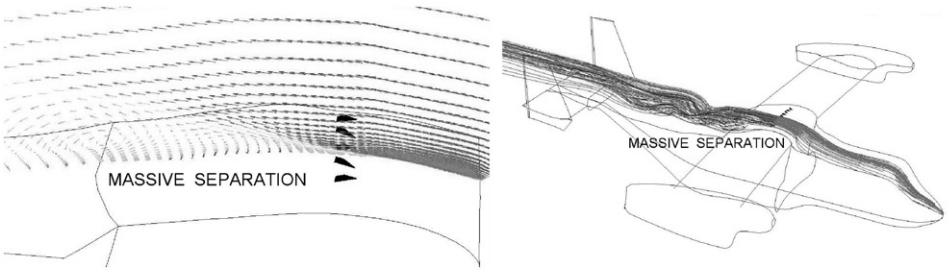

(b) 10 VGs with $\beta = \pm 20$ deg. located at ~32 h upstream of baseline separation (Configuration B).

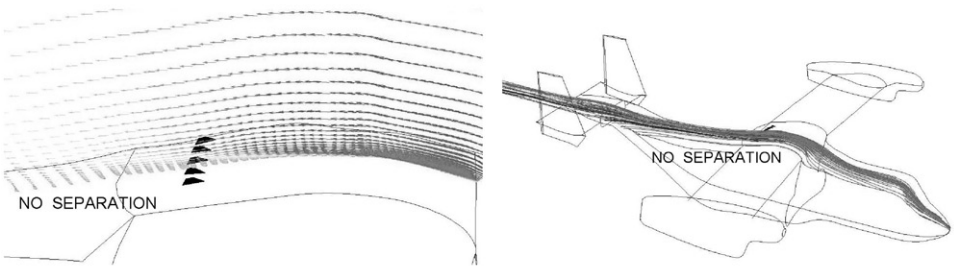

(c) 10 VGs with $\beta = \pm 9$ deg. located ~10 h upstream of baseline separation (Configuration E).

Fig. 31. Velocity vectors and particle traces over V-22 overwing fairing at $M_\infty = 0.345$ and $\alpha = 7^\circ$ [36]. (CFD based on the modified Baldwin–Lomax turbulence model).

low-profile VGs with $0.1 \leqslant h/\delta \leqslant 0.5$. Data analysis from both basic fluid dynamics and applied aerodynamics research reveals that the low-profile vortex generators are typically best for being applied to applications where flow-separation locations are relatively fixed and the generators can be placed reasonably close (less than $100\,h$) upstream of the baseline separation. Thus, the placement of low-profile VGs would be more critical than that of the conventional VGs. As a sign of their flow-control efficiency, the low-profile VGs use the approach of "minimal near-wall protuberances" to produce streamwise vortices just strong enough to overcome the baseline separation without unnecessarily persisting within the boundary layer once flow attachment is achieved. The rapid dissipation of streamwise vortices is highly desirable for flow-control application such as inside an S-duct inlet. Because of their substantially reduced height, device parameters such as the e/h, $\Delta z/h$, and β are generally increased substantially when compared with the classical design guideline for the conventional VGs in order to ensure the generation of sufficiently strong embedded streamwise vortices for flow-control purposes. Generally speaking, the counter-rotating VGs tend to be more effective in controlling 2D type of flow separation, while for 3D separation (such as those on

swept wings or inside compact-duct inlets) the co-rotating VGs tend to perform better.

The comparative flow-separation control studies in low-speed adverse pressure gradient flows show that embedded streamwise (longitudinal) vortices produced by low-profile VGs provide the most effective and efficient means of mitigating both 2D and 3D turbulent boundary-layer separations. Although the downstream coverage distance is reduced due to smaller VG size, by having them properly placed within their most effective range (between 5 and $30h$ upstream of baseline separation), the low-profile VGs with a device height of only 0.1–0.2δ are still highly effective in separation control. Investigation in supersonic flows reveals that the low-profile doublet (double ramps) VGs are highly effective in suppressing the shock-induced separation and significantly reduces the size of reverse flow region (separation bubble), resulting in sharper rise to pressure recovery. Although the boundary layer downstream becomes thinner and contains lower mixing losses, the suppression of the separation bubble decreases the extent of the lambda foot (oblique) shock system that results in a higher shock loss, whereas the passive cavity has exactly the opposite effect. Thus, the VGs appear to be more applicable for a supersonic diffuser because the shock-induced separation that usually limits diffuser performance is suppressed, allowing more subsonic pressure recovery to be obtained. In high-speed flows, the distance between the effective VG location and the baseline separation (ΔX_{VG}) seems to be over twice that of the low-speed flows, so as to allow streamwise vortices ample time (and space) to energize the low-momentum boundary-layer flow near the surface.

From basic vortex characterization research for flows over a flap plate, a correlation of vortex strength for various types of low-profile VGs against device Reynolds number for prediction purposes is developed using the concept of an effective device height. Test results covering up to $50h$ downstream of the device indicate that it is important to provide spaces between the vanes of counter-rotating VGs to reduce the mutual vortex interference (lead to faster vortex decay) and to prevent the device adversely affecting the boundary layer in adverse pressure gradient flows. Vortex decay is reasonably well predicted by a CFD method based on RANS solutions just downstream of the generators, but the prediction is less satisfactory further downstream. Device drag of counter-rotating VGs is satisfactorily predicted by CFD in zero pressure gradient. CFD also consistently underestimates the strength of peak vorticity just downstream of the device by as much as 40% in some cases. There might still be a need to improve numerical scheme and/or modeling of turbulence diffusion for a better simulation of VG-induced embedded streamwise vortices.

For flow-control applications on airfoils and wings, significant performance improvements are achieved through increased lift and/or reduced drag for a low-Reynolds number airfoil, high-lift airfoils, highly swept wings, and a transonic airfoil using various low-profile VGs. The wishbone VGs with $h/\delta \sim 0.3$ and $\Delta z/\delta \sim 19$ are shown to effectively control the laminar separation bubble on a Liebeck airfoil at low Reynolds numbers, providing up to 38% drag reduction. By keeping the device height relatively low ($h/\delta \sim 0.3$) and spacing relatively large ($\Delta z/h \sim 65$), it is possible to design low-drag VGs that produce a desirable eddy structure without prematurely generating a downstream turbulent boundary layer, resulting in greater drag reduction than those of larger VGs or transition trips. The device spacing parameter, $\Delta z/h \sim 65$, represents about 5 times the values typically used for turbulent flow-separation control. Counter-rotating VGs with device height as small as 0.18% of reference airfoil chord could effectively control flap separation at landing conditions for a three-element high-lift airfoil that are optimized for maximum lift. Separation alleviation on the flap could significantly increase the lift on the order of 10%, reduce the drag on the order of 50%, and increase L/D on the order of 100% at approach angle of attack. The optimum chordwise location of the VGs (25% flap chord) allows the devices to be hidden inside the flap well during aircraft cruise. Co-rotating wire VGs with a diameter (or device height) approximately equal to the local turbulent boundary layer's displacement thickness are effective in reducing the maximum lift-dependent drag factor by up to 16% on a 60° swept delta wing. The wire VGs could also delay the onset of buffet by almost 10% in lift coefficient. In addition, co-rotating vane VGs with $h/\delta \sim 0.5$ are effective in increasing L/D by about 5% when placed on the wing's leading edges or wing tips of a low-observable fighter aircraft model with a 40° wing-swept. Counter-rotating VGs with a device height equal to the boundary-layer displacement thickness and vane gaps spaced $1h$ apart produce over 20% increase in maximum lift force for a transonic airfoil at high subsonic speeds. A similar array of forwards wedges increase the maximum L/D by about 5%.

Performance enhancements using the low-profile VGs for non-airfoil applications include aircraft interior noise reduction, inlet flow distortion alleviation inside compact ducts, and a more efficient overwing fairing. Up to 5 dB reduction in interior noise on a Gulfstream III corporate aircraft at high subsonic cruise conditions is achieved through application of low-profile counter-rotating VGs with $h/\delta \sim 1/8$ on the aircraft canopy. The VGs delay shock-induced boundary-layer separation and attenuate the Kármán vortex street shed from the canopy shock wave, minimizing two major sources of noise. Theoretical investigations

through CFD and DOE optimization procedures demonstrate that inlet flow distortion alleviation inside a compact S-duct inlet could be achieved using co-rotating VGs with a device height on the order of boundary-layer momentum thickness. The VGs effectively manage the entire inlet flowfield by redistributing the near wall low-momentum fluids to suppress a pair of counter-rotating vortices lifting from the duct surface (3D flow separation), resulting in a reduction of engine face flow distortion by at least a factor of 3. A simplified CFD model of the VG vane could predict the effect of VGs in the S-duct inlet reasonably well a nd eliminate the need to model the device geometry, thereby resulting in a reduced computational cost. In addition, experimental results show that by properly placing the VGs inside an ultra-compact serpentine duct, total pressure recovery is increased by up to 5%, and DC(60) spatial distortion and RMS turbulence are decreased by as much as 50%. A gridding method recently introduced allows incorporation of the VGs onto an aircraft configuration for CFD design analysis. If the flow is separated on the overwing fairing of a V-22 aircraft, then a properly designed VG configuration could produce a small favorable effect on both lift and drag. The chordwise location and the device angle of incidence are found to be the two important parameters to achieve the desired separation alleviation.

In closing it should be noted that on top of their significant separation control effectiveness, practical advantages of low-profile vortex generators such as their inherent simplicity, low cost, and low device drag are also determined to be critically important for a wide range of applications. This is not to suggest that the low-profile VGs shall replace conventional VGs in all flow-control situations, but rather as a logical complement whenever the situations arise. Such as in flow-control situations where flow-separation locations are reasonably fixed and the generators can be placed relatively close upstream of the baseline separation. If properly implemented, the low-profile VGs could contribute substantially or play an important role in many real-life flow-control applications. For example, in addition to the flow-control application for the Gulfstream III aircraft cited in this paper, the design philosophy of low-profile VGs are being successfully used by at least two other aircraft currently in production: the Gulfstream V and Piper Malibu Meridian. The Gulfstream V aircraft, the winner of 1997 Collier Trophy, is able to achieve a higher maximum cruise speed as well as extend its operational range and exhibit better high-speed maneuver controllability by using the low-profile VGs on its outboard wings. The Piper Malibu Meridian prototype aircraft uses the flap-mounted low-profile VGs to easily pass the FAA stall certification requirement (below 61 kt).

References

[1] Gad-el-Hak M, Bushnell DM. Separation control: review. J Fluids Eng 1991;113:5–30.

[2] Chang PK. Control of flow separation. Washington, DC: Hemisphere Publishing Corporation, 1976.

[3] Haines AB. Know your flow: the key to better prediction and successful innovation. AIAA Paper 98-0221, 36th AIAA Aerospace Sciences Meeting and Exhibit, Reno, NV, January 12–15, 1998.

[4] Taylor HD. The elimination of diffuser separation by vortex generators. United Aircraft Corporation Report No. R-4012-3, June 1947.

[5] Schubauer GB, Spangenber WG. Forced mixing in boundary layers. J Fluid Mech, 1 1960;8:10–32.

[6] Bragg MB, Gregorek GM. Experimental study of airfoil performance with vortex generators. J Aircr 1987;24(5): 305–9.

[7] Pearcey HH. Shock induced separation and its prevention by design and boundary-layer control. Boundary layer and flow control, vol. 2. New York: Pergamon Press, 1961. p. 1166–344.

[8] ESDU Transonic Data Memorandum 93024—Vortex generators for control of shock-induced separation, Part 1: introduction and aerodynamics.

[9] Calarese W, Crisler WP, Gustsfson GL. Afterbody drag reduction by vortex generators. AIAA Paper 85-0354, AIAA 23rd Aerospace Sciences Meeting, Reno, NV, January 14–17, 1985.

[10] Brown AC, Nawrocki HF, Paley PN. Subsonic diffusers designed integrally with vortex generators. J Aircr 1968; 5(3):221–9.

[11] Kuethe AM. Effect of streamwise vortices on wake properties associated with sound generation. J Aircr 1972; 9(10):715–9.

[12] Rao DM, Kariya TT. Boundary-layer submerged vortex generators for separation control—an exploratory study. AIAA Paper 88-3546-CP, AIAA/ASME/SIAM/APS 1st National Fluid Dynamics Congress, Cincinnati, OH, July 25–28, 1988.

[13] Lin JC, Howard FG, Selby GV. Small submerged vortex generators for turbulent flow separation control. J Spacecr Rockets 1990;27(5):503–7.

[14] Lin JC, Howard FG, Bushnell DM, Selby GV. Investigation of several passive and active methods for turbulent flow separation control. AIAA Paper 90-1598, AIAA 21st Fluid Dynamics, Plasma Dynamics and Lasers Conference, Seattle, WA, June 18–20, 1990.

[15] Lin JC, Selby GV, Howard FG. Exploratory study of vortex-generating devices for turbulent flow separation control. AIAA Paper 91-0042, AIAA 29th Aerospace Sciences Meeting, Reno, NV, January 7-10, 1991.

[16] Lin JC. Control of turbulent boundary-layer separation using micro-vortex generators. AIAA Paper 99-3404, 30th AIAA Fluid Dynamics Conference, Norfolk, VA, June 28–July 1, 1999.

[17] Jenkins L, Gorton SA, Anders S. Flow control device evaluation for an internal flow with an adverse pressure gradient. AIAA Paper 2002-0266, 40th AIAA Aerospace Sciences Meeting and Exhibit, Reno, NV, January 14–17, 2002.

[18] McCormick DC. Shock–boundary layer interaction control with low-profile vortex generators and passive cavity. AIAA Paper 92-0064, 30th AIAA Aerospace Sciences Meeting and Exhibit, Reno, NV, January 6–9, 1992.
[19] Mounts JS, Barber TJ. Numerical analysis of shock-induced separation alleviation using vortex generators. AIAA Paper 92-0751, 30th AIAA Aerospace Sciences Meeting and Exhibit, Reno, NV, January 6–9, 1992.
[20] Ashill PR, Fulker JL, Hackett, KC. Research at DERA on sub boundary layer vortex generators (SBVGs). AIAA Paper 2001-0887, 39th AIAA Aerospace Sciences Meeting and Exhibit, Reno, NV, January 8–11, 2001.
[21] Ashill PR, Fulker JL, Hackett, KC. Studies of flows induced by sub boundary layer vortex generators (SBVGs). AIAA Paper 2002-0968, 40th AIAA Aerospace Sciences Meeting and Exhibit, Reno, NV, January 14–17, 2002.
[22] Yao C-S, Lin JC, Allan BG. Flowfield measurement of device-induced embedded streamwise vortex on a flat plate. AIAA Paper 2002-3162, 1st AIAA Flow Control Conference, St. Louis, MO, June 24–27, 2002.
[23] Allan BG, Yao C-S, Lin JC. Numerical simulation of vortex generator vanes and jets. AIAA Paper 2002-3160, 1st AIAA Flow Control Conference, St. Louis, MO, June 24–27, 2002.
[24] Kerho M, Hutcherson S, Blackwelder RF, Liebeck RH. Vortex generators used to control laminar separation bubbles. J Aircr 1993;30(3):315–9.
[25] Lin JC, Robinson SK, McGhee RJ, Valarezo WO. Separation control on high-lift airfoils via micro-vortex generators. J Aircr 1994;31(6):1317–23.
[26] Klausmeyer S, Papadakis M, Lin J. A flow physics study of vortex generators on a multi-element airfoil. AIAA Paper 96-0548, 34th AIAA Aerospace Sciences Meeting and Exhibit, Reno, NV, January 15–18, 1996.
[27] Ashill PR, Riddle GL. Control of leading-edge separation on a cambered delta wing. AGARD CP-548, March 1994. p 11-1–11-13.
[28] Ashill PR, Riddle GL, Stanley MJ. Control of three-dimensional separation on highly swept wings. ICAS-94-4.6.2, September 1994.
[29] Ashill PR, Riddle GL, Stanley MJ. Separation control on highly swept wings with fixed or variable camber. Aeronaut J. 1995;99(988):317–27.
[30] Ashill PR, Fulker JL. A review of flow control research at DERA. Mechanics of Passive and Active Flow Control, IUTAM Symposium, Gottingen, Germany, September 7–11, 1998. p. 43–56.
[31] Langan KJ, Samuels JJ. Experimental investigation of maneuver performance enhancements on an advanced fighter/attack aircraft. AIAA Paper 95-0442, AIAA 33rd Aerospace Sciences Meeting, Reno, NV, January 9–12, 1995.
[32] Holmes AE, Hickey PK, Murphy WR, Hilton DA. The application of sub-boundary layer vortex generators to reduce canopy Mach rumble interior noise on the Gulfstream III. AIAA Paper 87-0084, AIAA 25th Aerospace Sciences Meeting, Reno, NV, January 12–15, 1987.
[33] Anabtawi AJ, Blackwelder RF, Lissaman PBS, Liebeck RH. An experimental investigation of boundary layer ingestion in a diffusing S-duct with and without passive flow control. AIAA Paper 99-0739, 37th AIAA Aerospace Sciences Meeting and Exhibit, Reno, NV, January 11–14, 1999.
[34] Anderson BH, Miller DN, Yagle PJ, Truax PP. A study on MEMS flow control for the management of engine face distortion in compact inlet systems. Third ASME/JSME Joint Fluids Engineering Conference, ASME Paper FEDSM99-9620, July 1999.
[35] Hamstra JW, Miller DN, Truax PP, Anderson BH, Wendt BJ. Active inlet flow control technology demonstration. ICAS-2000-6.11.2, 22nd International Congress of the Aeronautical Sciences, Harrogate, UK, August 27–September 1, 2000.
[36] Tai TC. Effect of micro-vortex generators on V-22 aircraft forward-flight aerodynamics. AIAA Paper 2002-0553, 40th AIAA Aerospace Sciences Meeting and Exhibit, Reno, NV, January 14–17, 2002.
[37] Wheeler GO. Means of maintaining attached flow of a flow medium. US Patent 4455045, 1984.
[38] Wheeler GO. Low drag vortex generators. US Patent 5058837, 1991.
[39] Bender EE, Anderson BH, Yagle PJ. Vortex generator modeling for Navier–Stokes codes. Third ASME/JSME Joint Fluids Engineering Conference, ASME Paper FEDSM99-6919, July 1999.
[40] Jesperson DC. Parallelism and OVERFLOW. NASA TP NAS-98-013, October 1998.
[41] Valarezo WO. Topics in high-lift aerodynamics. AIAA Paper 93-3136, AIAA 24th Fluid Dynamics Conference, Orlando, FL, July 6–9, 1993.
[42] Woodward DS, Hardy BC, Ashill PR. Some types of scale effect in low-speed high-lift flows. ICAS-88-4.9.3, August-September 1988.
[43] Kuchemann D. The aerodynamic design of aircraft. Oxford: Pergamon Press Ltd, 1978.
[44] Anderson BH, Huang PS, Paschal WA, Cavatorta E. Study of vortex flow control of inlet distortion. J Propulsion Power 1992;8(6):1266–72.
[45] Anderson BH, Gibb J. Vortex generator installation studies on steady state and dynamic distoration. AIAA Paper 96-3279, 32nd AIAA/ASME/SAE/ASEE Joint Propulsion Conference, Lake Buena Vista, FL, July 1–3, 1996.
[46] Box EP, Hunter WG, Hunter JS. Statistics for experimenters. New York: John Wiley & Sons, 1978.
[47] Thomas JL, Krist ST, Anderson WK. Navier-Stokes computations of vortical flows over low-aspect-ratio wings. AIAA J 1990;28(2):205–12.
[48] Sorenson RL. The 3DGRAPE book: theory, users' manual, examples. NASA TM 102224, July 1989.
[49] Flores J, Holst TL. Numerical solution of the Navier–Stokes equations for complex configurations. Lecture Series in Computational Fluid Dynamics, University of Tennessee Space Inst., Tulahoma, TN, March 1988.